Supplementary information for

An Alveolata secretory machinery adapted to parasite-host cell invasion

Authors

Eleonora Aquilini[1§], Marta Mendonça Cova[1§], Shrawan Kumar Mageswaran[2], Nicolas Dos Santos Pacheco[1], Daniela Sparvoli[1,3], Diana Marcela Penarete-Vargas[1], Rania Najm[1], Arnault Graindorge[1], Catherine Suarez[1], Marjorie Maynadier[1], Laurence Berry-Sterkers[1], Serge Urbach[4], Pilar Ruga Fahy[5], Amandine N. Guérin[6], Boris Striepen[6], Jean-François Dubremetz[1], Yi-Wei Chang[2], Aaron Turkewitz[3], Maryse Lebrun[1*]

[§]These authors contributed equally to the work

*corresponding author: maryse.lebrun@umontpellier.fr

This file includes:

- Extended data Figures 1 to 11
- Supplementary Table 1
- Supplementary Text
- Captions for Supplementary Tables 2 to 4
- Caption for Extended Data 1
- Supplementary Methods
- Supplementary References

Supplementary Figures

Extended Data Fig. 1| Amino acid sequence alignments and phylogenetic analyses

a, b, c, d, Maximum likelihood phylogenetic trees based on *Alveolata* non discharge (Nd) Nd6 (a) Nd9 (b) NdP1 (c) and NdP2 (d) protein sequences. Asterisks indicate two homologous genes in the same species. The scale bar represents the branch length values. Amino acids sequences, accession number and alignments used to generate phylogenetic tree of Nd6, Nd9, NdP1 and NdP2 are presented in Extended Data 1.

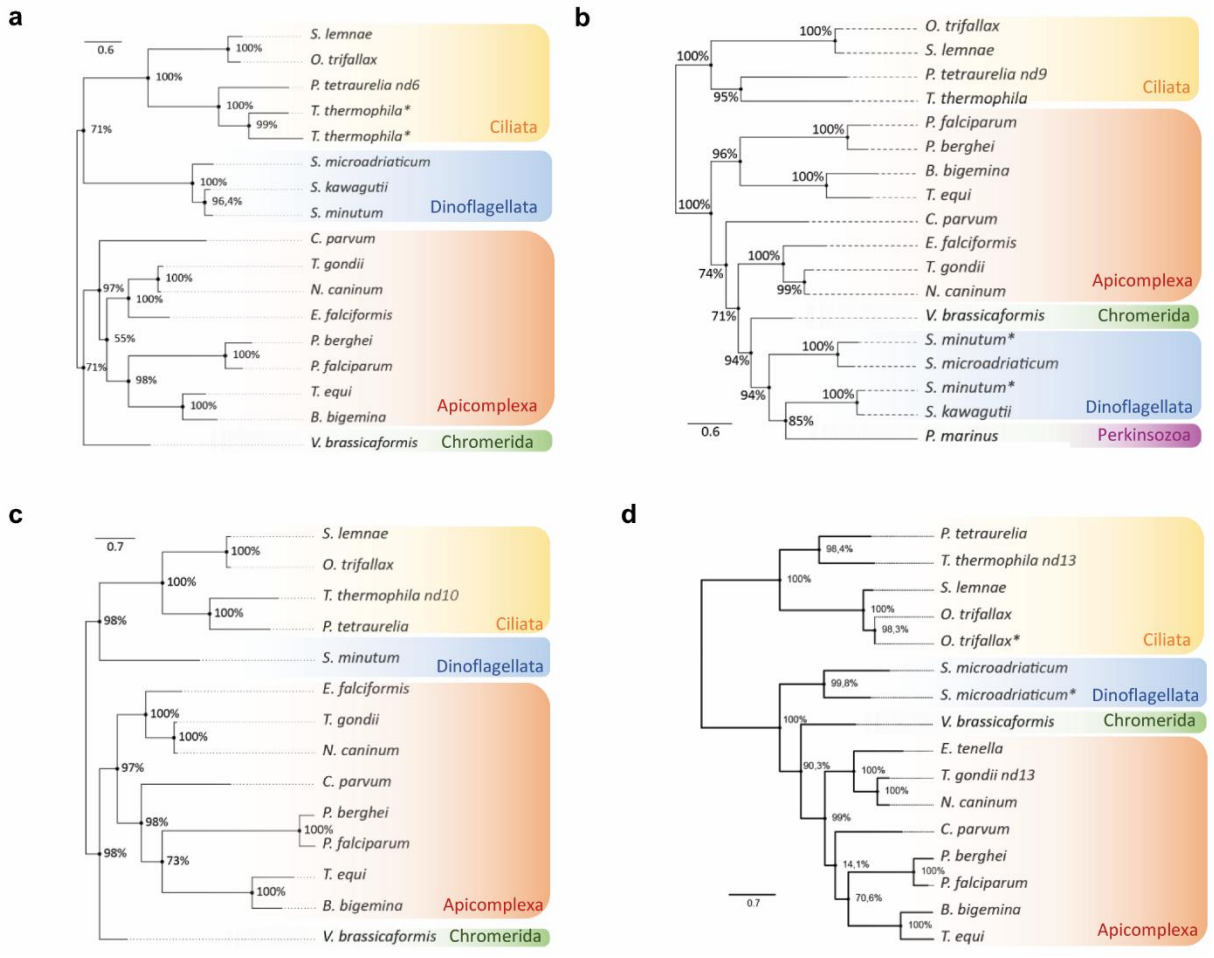

Extended Data Fig. 2 | Generation of *Tgnd6*-iKD and *Tgnd9*-iKD.

a, Strategy for conditional depletion of *Tg*Nd6 (TGGT1_248640) using the Auxin-inducible degron system. **b**, Integration PCRs showing double homologous recombination at the 5' (top) and at the 3' (bottom) of the *Tgnd6* locus. **c**, Strategy for conditional depletion of *Tg*Nd9 (TGGT1_249730) using the Tet-OFF system. **d**, Integration PCRs showing double homologous recombination at the 3' (top) and at the 5' (bottom) of the *Tgnd9* locus. **e**, Immunoblot of *Tgnd6*-iKD ± IAA (top) and *Tgnd9*-iKD ± ATc (bottom) showing the timing for protein depletion. ROP5, loading control. Ctrl: *ΔKu80-Tir1* (upper panel) and *ΔKu80-TaTi* (lower panel). **f**, IFA of *Tgnd6*-iKD shows depletion of *Tg*Nd6 after 24 hours IAA treatment (top right), IFA of *Tgnd9*-iKD shows depletion of *Tg*Nd9 after 72 hours ATc treatment (bottom right). Red, anti-ARO. Green, anti-HA. **g,** Detergent extraction profile of *Tg*ND6 and *Tg*ND9 after solubilization of HA-tagged *Tg*Nds parasites with Tris 1mM, 1% TritonX-100 or 1% SDS.

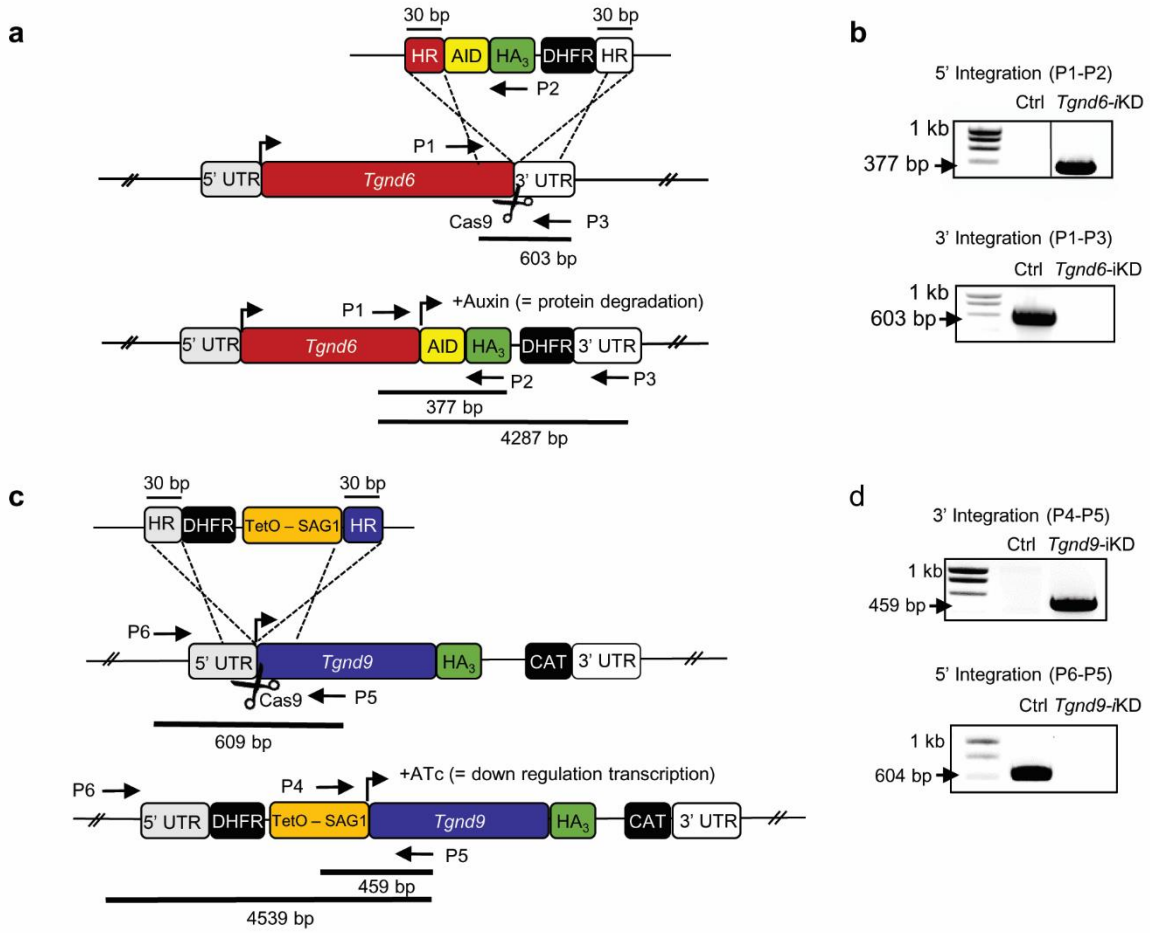
a
30 bp
30 bp
HR
AID
HA3
DHFR
HR
P2
P1
5' UTR
Tgnd6
3' UTR
Cas9
P3
603 bp
P1
+Auxin (= protein degradation)
5' UTR
Tgnd6
AID
HA3
DHFR
3' UTR
P2
P3
377 bp
4287 bp
b
5' Integration (P1-P2)
Ctrl
Tgnd6-iKD
1 kb
377 bp
3' Integration (P1-P3)
Ctrl
Tgnd6-iKD
1 kb
603 bp
c
30 bp
30 bp
HR
DHFR
TetO – SAG1
HR
P6
5' UTR
Tgnd9
HA3
CAT
3' UTR
Cas9
P5
609 bp
P6
P4
+ATc (= down regulation transcription)
5' UTR
DHFR
TetO – SAG1
Tgnd9
HA3
CAT
3' UTR
P5
459 bp
4539 bp
d
3' Integration (P4-P5)
Ctrl
Tgnd9-iKD
1 kb
459 bp
5' Integration (P6-P5)
Ctrl
Tgnd9-iKD
1 kb
604 bp

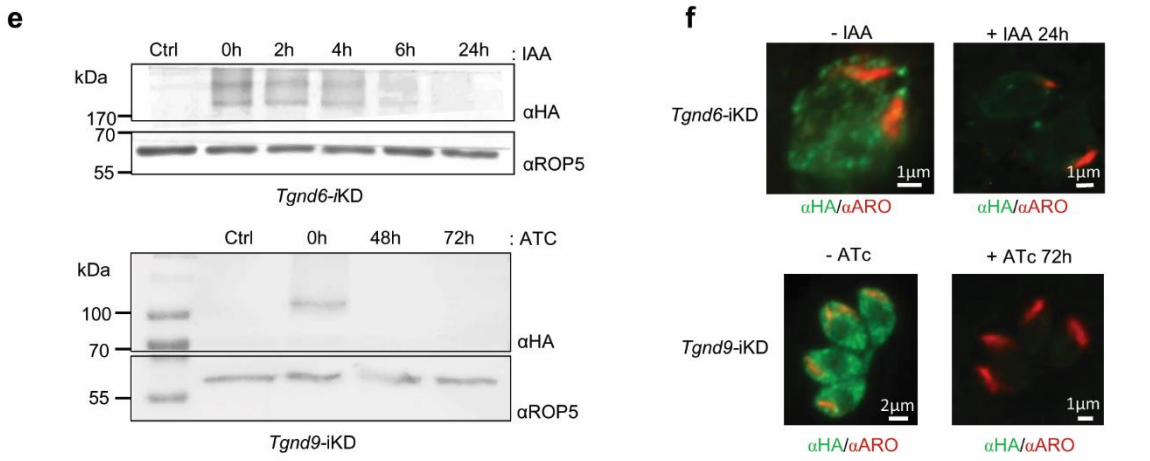
e
Ctrl
0h
2h
4h
6h
24h
: IAA
kDa
170
70
55
αHA
αROP5
Tgnd6-iKD
Ctrl
0h
48h
72h
: ATC
kDa
100
70
55
αHA
αROP5
Tgnd9-iKD
f
- IAA
+ IAA 24h
Tgnd6-iKD
1µm
1µm
αHA/αARO
αHA/αARO
- ATc
+ ATc 72h
Tgnd9-iKD
2µm
1µm
αHA/αARO
αHA/αARO

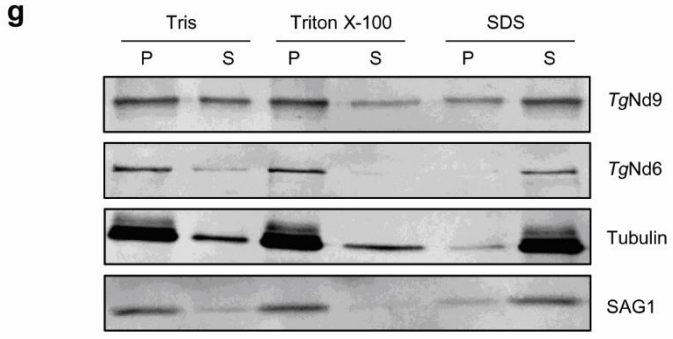
g
Tris
Triton X-100
SDS
P
S
P
S
P
S
TgNd9
TgNd6
Tubulin
SAG1

47

Extended Data Fig. 3 | Depletion of Nd6 or Nd9 in *T. gondii* parasites does not affect replication, egress, gliding motility nor attachment.

a, Plaque assay. Left: *ΔKu80-Tir1* (Ctrl) ± IAA vs *Tgnd6*-iKD ± IAA. Right: *ΔKu80-TaTi* (Ctrl) ± ATc vs *Tgnd9*-iKD ± ATc. 7 dpi lysis plaque areas were measured. Mean value of plaque area ± SD (n=26 for *ΔKu80-Tir1* -IAA, n=33 for *ΔKu80-Tir1* +IAA, n=23 for *Tgnd6*-iKD -IAA, and n=27 for *Tgnd6*-iKD +IAA; n=13 for *ΔKu80-TaTi* -ATc, n=15 for *ΔKu80-TaTi* +ATc, n=15 for *Tgnd9*-iKD -ATc, no plaques were observed for *Tgnd9*-iKD +ATc). **b**, Intracellular replication. Left: *ΔKu80-Tir1* (Ctrl) and *Tgnd6*-iKD ± IAA. Right: *ΔKu80-TaTi* (Ctrl) and *Tgnd9*-iKD ± ATc. The percentage of vacuoles containing 2, 4, 8, 16 or 32 parasites was determined for 200 vacuoles. Means ± SD, n=3 biological replicates, from a representative experiment out of 3 independent assays. **c**, Percentage of egressed vacuoles. Left: *ΔKu80-Tir1* (Ctrl) and *Tgnd6*-iKD ± IAA. Right: *ΔKu80-TaTi* (Ctrl) and *Tgnd9*-iKD ± ATc. Parasite egress was induced 30 hours post-invasion by addition of A23187 (3 μM) for 8 min. IFA with anti-GRA3 antibodies. Egress events (GRA3 in the PV) were quantified for 30 vacuoles. Means ± SD, n=3 biological replicates, from a representative experiment out of 2 independent assays. **d**, Conoid protrusion assay. The graph represents the percentage of protruded conoids induced by 5 μM A23187, or DMSO as control. Mean ± SD. n=3 biological replicates, from a representative experiment out of 3 independent assays. **e**, Gliding assays were performed with *ΔKu80-Tir1* (Ctrl) and *Tgnd6*-iKD parasite lines ± IAA 24h (left) and *ΔKu80-TaTi* (Ctrl) and *Tgnd9*-iKD parasite lines ± ATc 72h (right). Trails were revealed by IFA using anti-SAG1 antibodies. Scale bar=10μm. **f**, Quantification of parasite motility by time-lapse video microscopy as previously defined[1]. Data are plotted as a percentage of the three well-described circular, helical and twirling movements. Values represent mean ± SD of minimum 3 movies. **g,** Quantification of attachment on glutaraldehyde fixed host cell. As control of microneme

secretion-dependent attachment, parasites were treated with BAPTA-AM. **h,** Quantification of rhoptry secretion by e-vacuoles assay. *Tgnd6*-iKD was compared to the background line *Δku80-Tir1* ± IAA 24h and *Tgnd9*-iKO was compared to the background line *Δku80-TATi* ± Atc 72h. (f-h) Mean ± SD of n=3 biological replicates of one experiment. (**a**-**h**) The significance of the results was assessed using a parametric paired t-test (Student's one-tailed *t*-test). **** *p*-value < 0.0001, *** *p*-value < 0.001, ** *p*-value < 0.01, * *p*-value < 0.05, ns = non-significant.

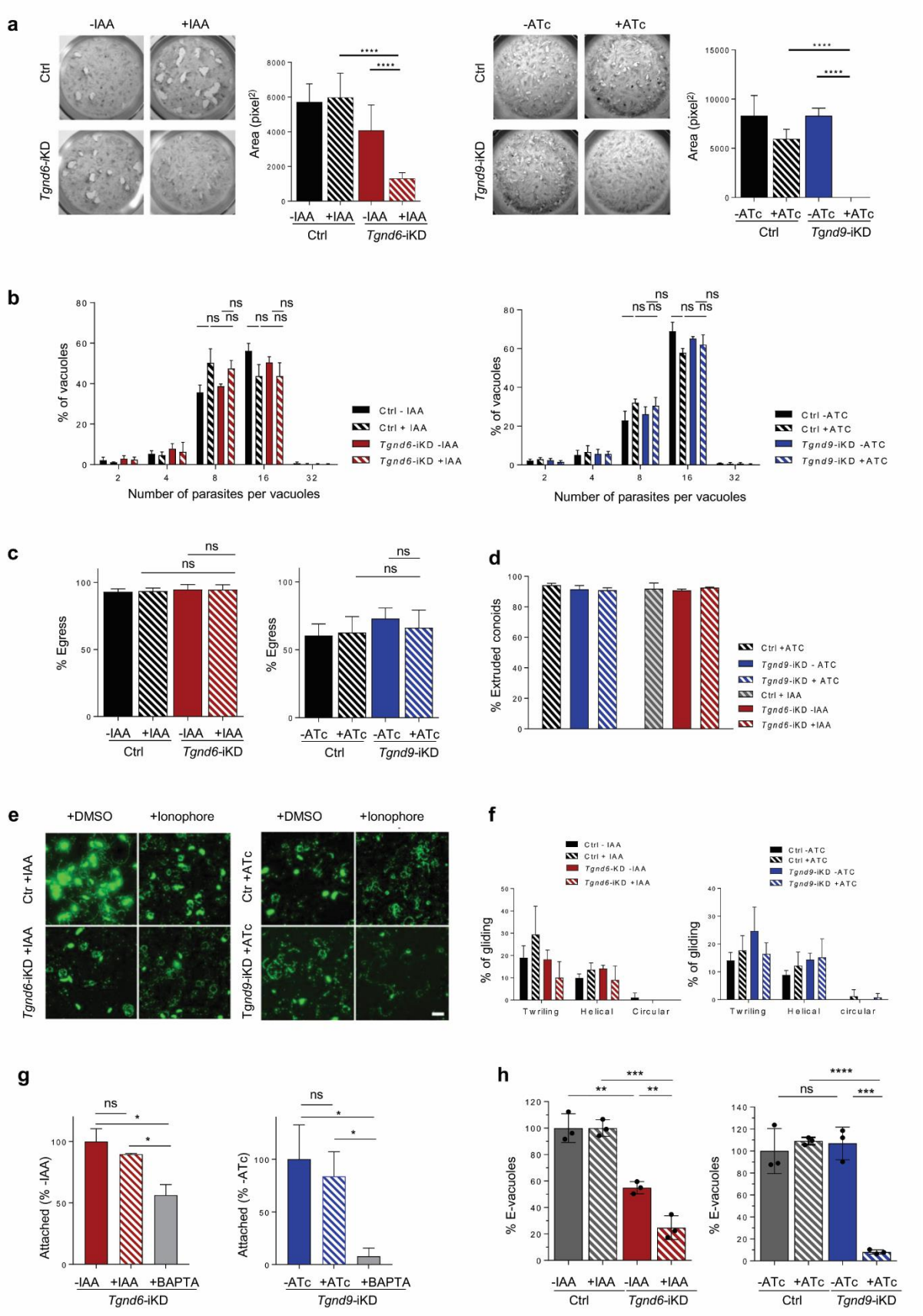
a
-IAA
+IAA
Ctrl
Tgnd6-iKD
Area (pixel²)
-IAA +IAA -IAA +IAA
Ctrl
Tgnd6-iKD
-ATc
+ATc
Tgnd9-iKD
-ATc +ATc -ATc +ATc
Ctrl
Tgnd9-iKD
b
% of vacuoles
Number of parasites per vacuoles
Ctrl - IAA
Ctrl + IAA
Tgnd6-iKD -IAA
Tgnd6-iKD +IAA
Ctrl -ATC
Ctrl +ATC
Tgnd9-iKD -ATC
Tgnd9-iKD +ATC
c
% Egress
d
% Extruded conoids
e
+DMSO
+Ionophore
Ctr +ATc
Tgnd9-iKD +ATc
f
% of gliding
Twriling
Helical
Circular
g
Attached (% -IAA)
Attached (% -ATc)
-IAA +IAA +BAPTA
Tgnd6-iKD
-ATc +ATc +BAPTA
Tgnd9-iKD
h
% E-vacuoles

79

80

Extended Data Fig. 4 | Secretory organelle biogenesis and positioning is not affected in *Tgnd6*-iKD and *Tgnd9*-iKD.

a, b, IFA using anti-ARO antibodies (rhoptry marker) and anti-MIC2 (microneme marker) on *Tgnd6*-iKD parasites ± IAA 24h (**a**) and on *Tgnd9*-iKD parasites ± ATc 72h (**b**). Scale bar=1µm. **c**, **d**, Electron microscopy images showing the apical complex of extracellular tachyzoites of *Tgnd6*-iKD +IAA 24h (**c**) and of *Tgnd9*-iKD +ATc 72h (**d**). Rh B = rhoptry bulb, Rh N = rhoptry neck, Co = conoid, m = microneme. Bar = 500 nm.

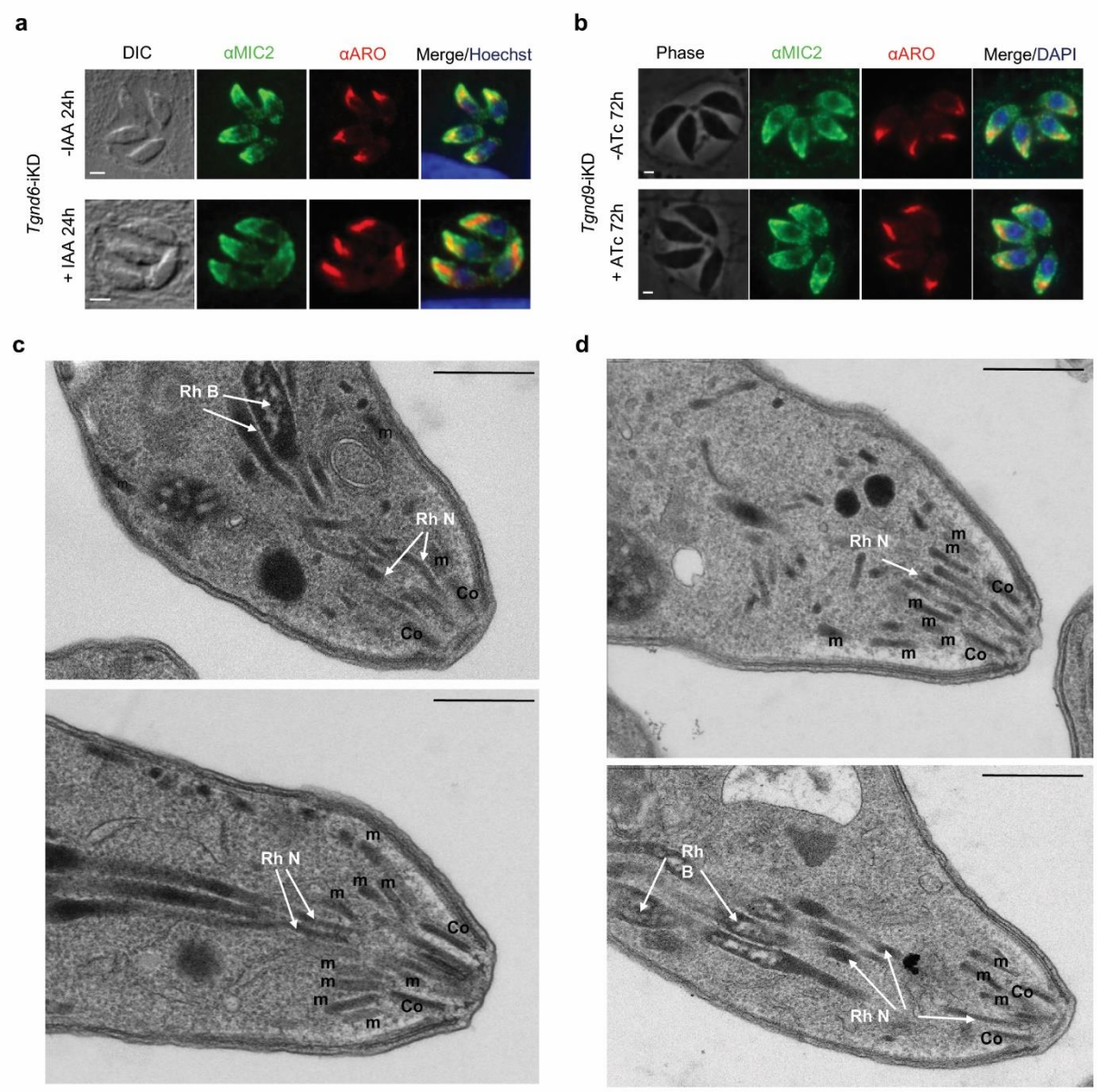

Extended Data Fig. 5 | Generation of *Pfnd9*-iKO

a, Strategy for conditional depletion of *Pf*Nd9 (PF3D7_1232700)) using the DiCre system, allowing the simultaneously tagging of the gene by a triple HA. **b**, Integration PCRs showing double homologous recombination at the 5' end (top panel) and at the 3' end (middle panel) of the *Pfnd9* locus. In the bottom panel, PCR demonstrating the absence of the wt locus in the floxed clonal population. **c,** PCRs showing efficient excision of the *Pfnd9* locus upon addition of rapamycin. **d,** Immunoblot on parasite lysates from *Pfnd9*-iKO mutant parasites. We could not detect the protein by IFA and only observed a faint band at the expected size in late schizonts by Western blot, both consistent with the very low transcript level of *PfNd9* (Plasmodb.org). **e,** Representative images from the time lapse video microscopy of merozoites egressing from schizonts in the DMSO control and in the rapamycin-treated *Pfnd9*-iKO parasites. Relative time shown in minutes.

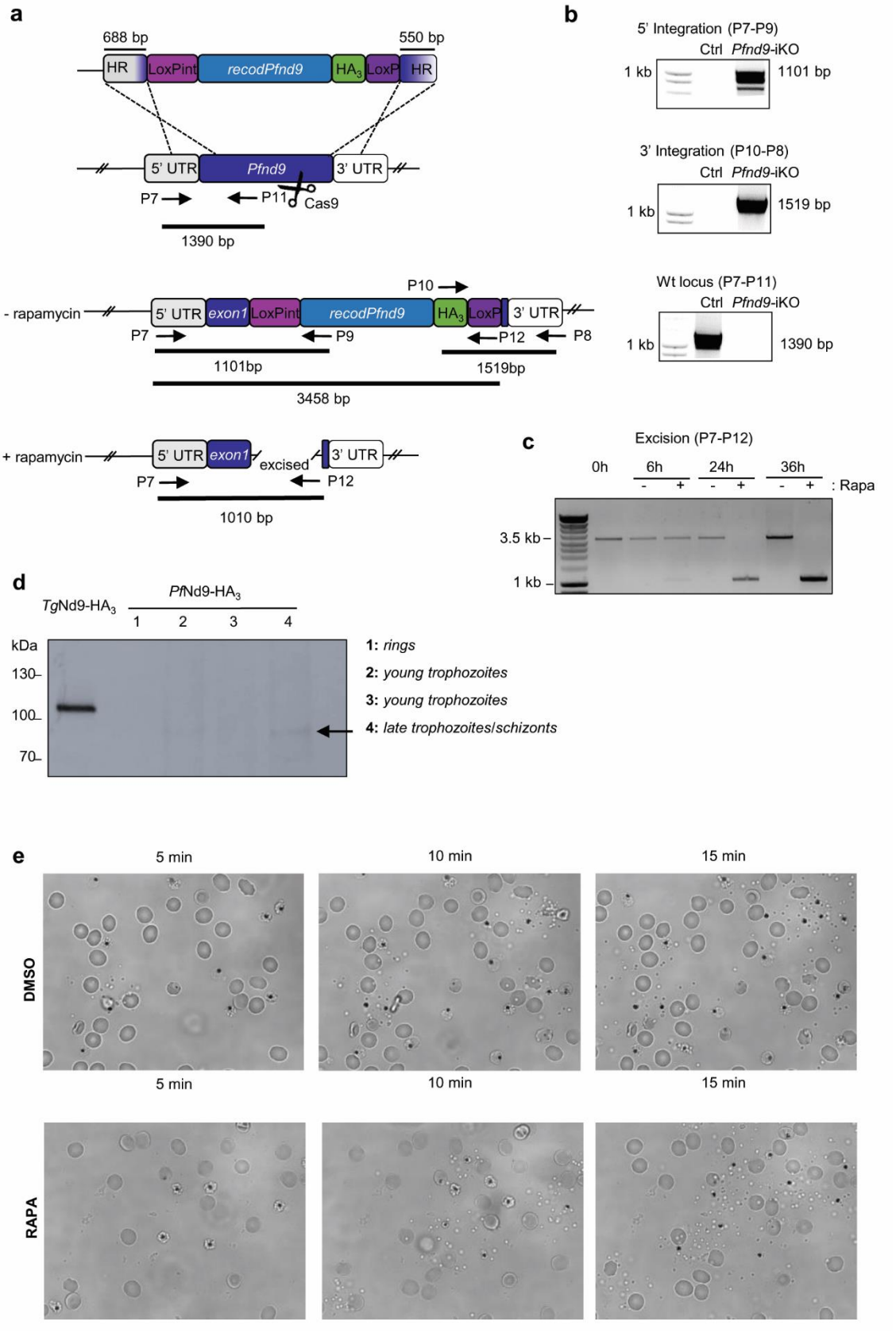
a
688 bp
550 bp
HR
LoxPint
recodPfnd9
HA3
LoxP
HR
5' UTR
Pfnd9
3' UTR
P7
P11
Cas9
1390 bp
P10
- rapamycin
5' UTR
exon1
LoxPint
recodPfnd9
HA3
LoxP
3' UTR
P7
P9
P12
P8
1101bp
1519bp
3458 bp
+ rapamycin
5' UTR
exon1
excised
3' UTR
P7
P12
1010 bp
b
5' Integration (P7-P9)
Ctrl
Pfnd9-iKO
1 kb
1101 bp
3' Integration (P10-P8)
Ctrl
Pfnd9-iKO
1 kb
1519 bp
Wt locus (P7-P11)
Ctrl
Pfnd9-iKO
1 kb
1390 bp
c
Excision (P7-P12)
0h
6h
24h
36h
- + - + - +
: Rapa
3.5 kb
1 kb
d
TgNd9-HA3
PfNd9-HA3
1 2 3 4
kDa
130
100
70
1: rings
2: young trophozoites
3: young trophozoites
4: late trophozoites/schizonts
e
5 min
10 min
15 min
DMSO
5 min
10 min
15 min
RAPA

Extended Data Fig. 6 | Generation of *Tgnp1*-iKD and *Tgndp2*-iKD

a, Strategy for conditional depletion of *Tg*NdP1 (TGGT1_222660) using the Tet-OFF system. **b**, PCRs confirming integration events (double homologous recombination) at the 5' end (top panel) and at the 3' end (bottom panel) at the *Tgnp1* locus. **c,** Strategy for conditional depletion of *Tg*NdP2 (TGGT1_ 316730) using the Auxin-inducible degron system. **d**, PCRs confirming integration events (double homologous recombination) at the 5' end (top panel) and at the 3' end (bottom panel) at the *Tgnp2* locus. **e,** Immunoblot of *Tgndp1*-iKD +ATc and *Tgndp2*-iKD +IAA showing proteins depletion. ROP5, loading control. Ctrl: *ΔKu80-TATi* (left) and *ΔKu80-Tir1* (right). **f,** IFA of *Tgndp1*-iKD shows depletion of *Tg*NdP1 after 48 hours ATc treatment (left), IFA of *Tgndp2*-iKD shows depletion of *Tg*NdP2 after 24 hours IAA treatment (right).

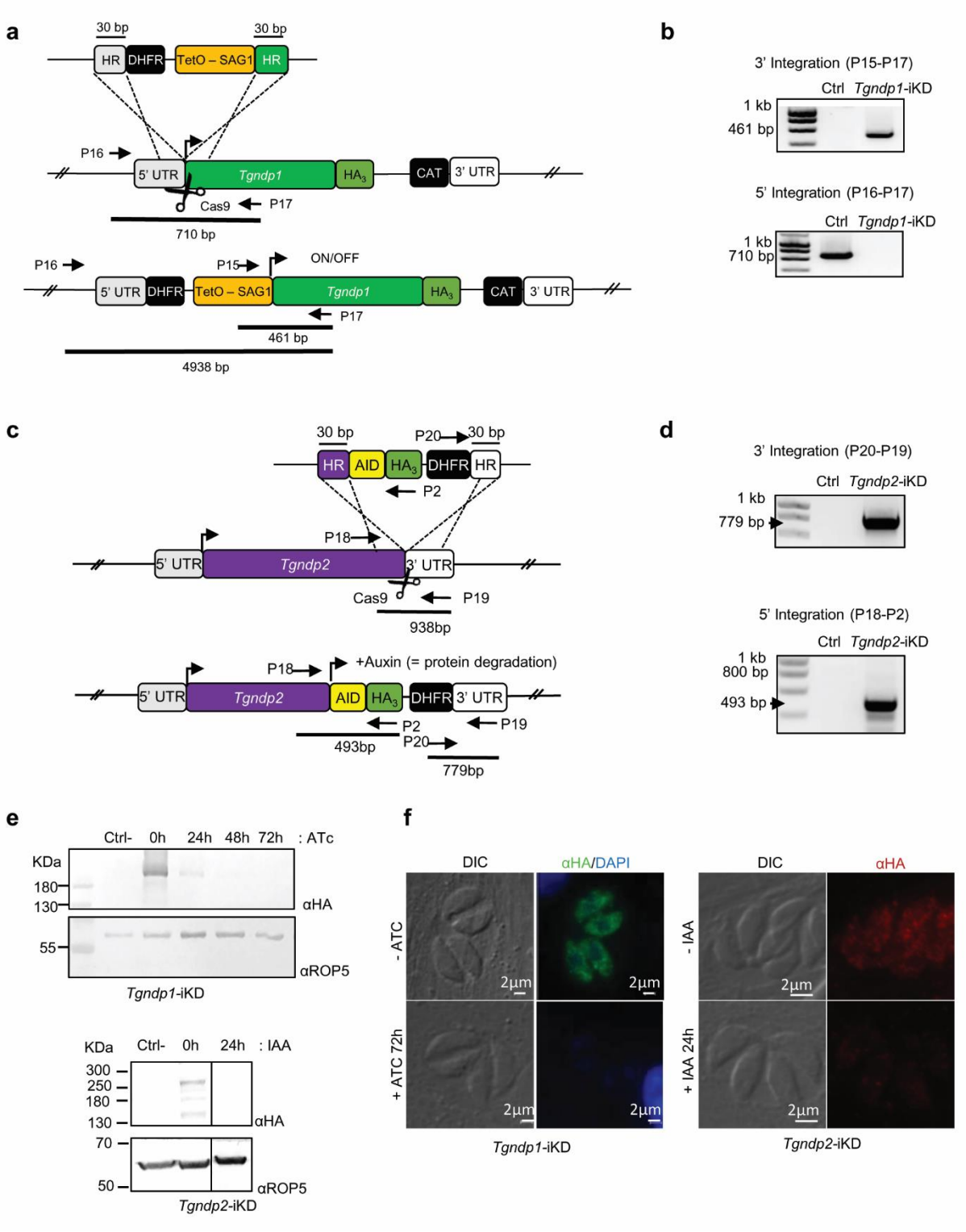
a
30 bp
30 bp
HR
DHFR
TetO – SAG1
HR
P16
5' UTR
Tgndp1
HA3
CAT
3' UTR
Cas9
P17
710 bp
P16
P15
ON/OFF
5' UTR
DHFR
TetO – SAG1
Tgndp1
HA3
CAT
3' UTR
P17
461 bp
4938 bp
b
3' Integration (P15-P17)
Ctrl
Tgndp1-iKD
1 kb
461 bp
5' Integration (P16-P17)
Ctrl
Tgndp1-iKD
1 kb
710 bp
c
30 bp
P20
30 bp
HR
AID
HA3
DHFR
HR
P2
P18
5' UTR
Tgndp2
3' UTR
Cas9
P19
938bp
P18
+Auxin (= protein degradation)
5' UTR
Tgndp2
AID
HA3
DHFR
3' UTR
P2
P19
493bp
P20
779bp
d
3' Integration (P20-P19)
Ctrl
Tgndp2-iKD
1 kb
779 bp
5' Integration (P18-P2)
Ctrl
Tgndp2-iKD
1 kb
800 bp
493 bp
e
Ctrl-
0h
24h
48h
72h
: ATc
KDa
180
130
αHA
55
αROP5
Tgndp1-iKD
KDa
Ctrl-
0h
24h
: IAA
300
250
180
130
αHA
70
50
αROP5
Tgndp2-iKD
f
DIC
αHA/DAPI
- ATC
+ ATC 72h
2µm
DIC
αHA
- IAA
+ IAA 24h
2µm
Tgndp1-iKD
Tgndp2-iKD

115

116

Extended Data Fig. 7 | Depletion of NdP1 or NdP2 in *T. gondii* parasites does not affect replication, egress, gliding motility, nor attachment.

a, Plaque assay. Top: *ΔKu80-TaTi* (Ctrl) ± ATc vs *Tgndp1*-iKD ± ATc. Bottom: *ΔKu80-Tir1* (Ctrl) ± IAA vs *Tgndp2*-iKD ± IAA. Mean value of plaque area ± SD (n=25 for *ΔKu80-TaTi* -ATc, n=21 for *ΔKu80-TaTi* +ATc, n=18 for *Tgndp10*iKD -ATc, no plaques were observed for *Tgndp1*-iKD +ATc, n=8 for *ΔKu80-Tir1* -IAA, n=10 for *ΔKu80-Tir1* +IAA, n=11 for *Tgndp2*-iKD –IAA, and n=16 for *Tgndp2*-iKD +IAA). **b**, IFA using anti-ROP5 and anti-ARO antibodies (rhoptry markers), and anti-MIC2 (microneme marker) on *Tgndp1*-iKD +ATc 72h and *Tgndp2*-iKD +IAA 24h. Scale bar=1µm**. c**, Intracellular replication. *ΔKu80-TaTi* (Ctrl) vs *Tgndp1*-iKD ±ATc and *ΔKu80-Tir1* (Ctrl) vs *Tgndp2*-iKD ±IAA. The percentage of vacuoles containing 2, 4, 8, 16 or 32 parasites was determined for 200 vacuoles. Means ± SD, n=3 biological replicates, from a representative experiment out of 3 independent assays. **d**, Percentage of egressed vacuoles. *ΔKu80-TaTi* (Ctrl) vs *Tgndp1*-iKD ± ATc and *ΔKu80-Tir1* (Ctrl) vs *Tgndp2*-iKD ± IAA. Parasite egress was induced 30 hours post-invasion by addition of A23187 (3 µM) for 8 min. IFA with anti-GRA3 antibodies. Egress events (GRA3 in the PV) were quantified for >200 vacuoles. Means ± SD, n=3 biological replicates, from one experiment. **e**, Conoid protrusion assay. The graph represents the percentage of protruded conoids induced by 5 µM A23187, and DMSO as control. Mean ± SD. n=3 biological replicates, from a representative experiment out of 3 independent assays. **f,** Gliding assays comparing *ΔKu80-TaTi* (Ctrl) vs *Tgndp1*-iKD parasite lines ± ATc 72h or comparing *ΔKu80-Tir1* (Ctrl) vs *Tgndp2*-iKD ± IAA 24h. Trails were revealed by IFA using anti-SAG1 antibodies. **g** Quantification of parasite motility by time-lapse video microscopy. Data are plotted as a percentage of the three well-described circular, helical and twirling movements. Values represent mean ± SD of minimum 3 movies. **h,** Quantification of attachment on glutaraldehyde fixed host cell. As control of microneme secretion-dependent attachment, parasites were treated with BAPTA-AM. **i,** Immunoblot

showing microneme secretion assessed by the release of the processed form of AMA1 (arrow=processed/secreted *Tg*AMA1) in *Tgndp1*-iKD ± ATc 72h and *Tgndp2*-iKD ± IAA 24h. Ctrl= *ΔKu80-Tir1*+IAA 24. P = pellet, Sup = supernatant, Sup ind = propanolol-induced supernatant. GRA3, loading control. **j,** Quantification of rhoptry secretion by e-vacuoles assay in *Tgndp1*-iKD ±ATc 72h. (g and j) Mean ± SD of n=3 biological replicates of one experiment. (a, c-e, g, h and j) The significance of the results was assessed using a parametric paired t-test (Student's one-tailed *t*-test). **** *p*-value < 0.0001, *** *p*-value < 0.001, ** *p*-value < 0.01, * *p*-value < 0.05, ns = non-significant.

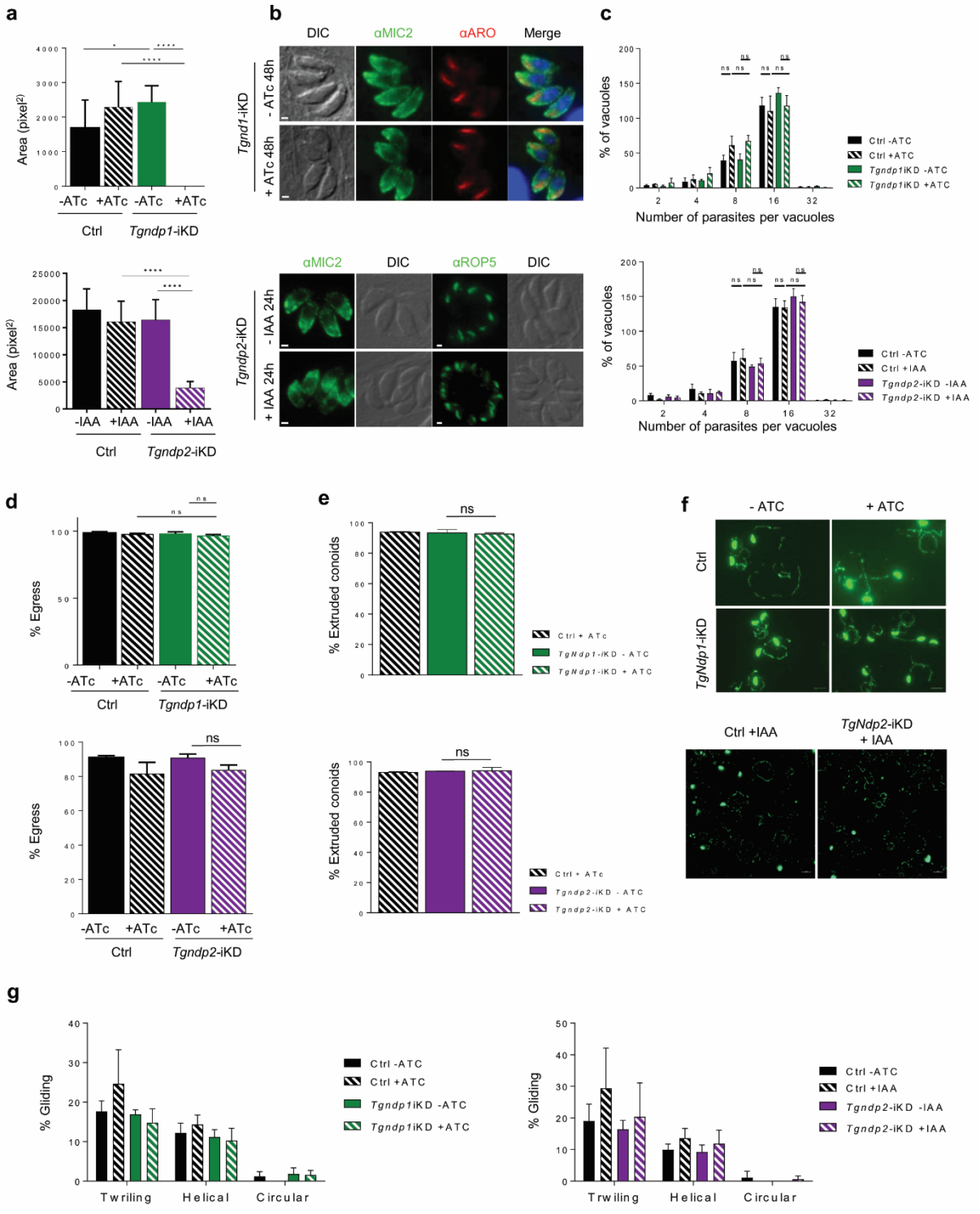
a
b
c
Area (pixel²)
-ATc +ATc -ATc +ATc
Ctrl
Tgndp1-iKD
DIC
αMIC2
αARO
Merge
Tgnd1-iKD
- ATc 48h
+ ATc 48h
% of vacuoles
Number of parasites per vacuoles
Ctrl -ATC
Ctrl +ATC
Tgndp1iKD -ATC
Tgndp1iKD +ATC
-IAA +IAA -IAA +IAA
Tgndp2-iKD
αROP5
Tgndp2-iKD
- IAA 24h
+ IAA 24h
Ctrl +IAA
Tgndp2-iKD -IAA
Tgndp2-iKD +IAA
d
e
f
% Egress
% Extruded conoids
ns
Ctrl + ATc
TgNdp1-iKD - ATC
TgNdp1-iKD + ATC
Tgndp2-iKD - ATC
Tgndp2-iKD + ATC
- ATC
+ ATC
Ctrl
TgNdp1-iKD
Ctrl +IAA
TgNdp2-iKD
+ IAA
g
% Gliding
Twriling
Helical
Circular
Trwiling

151

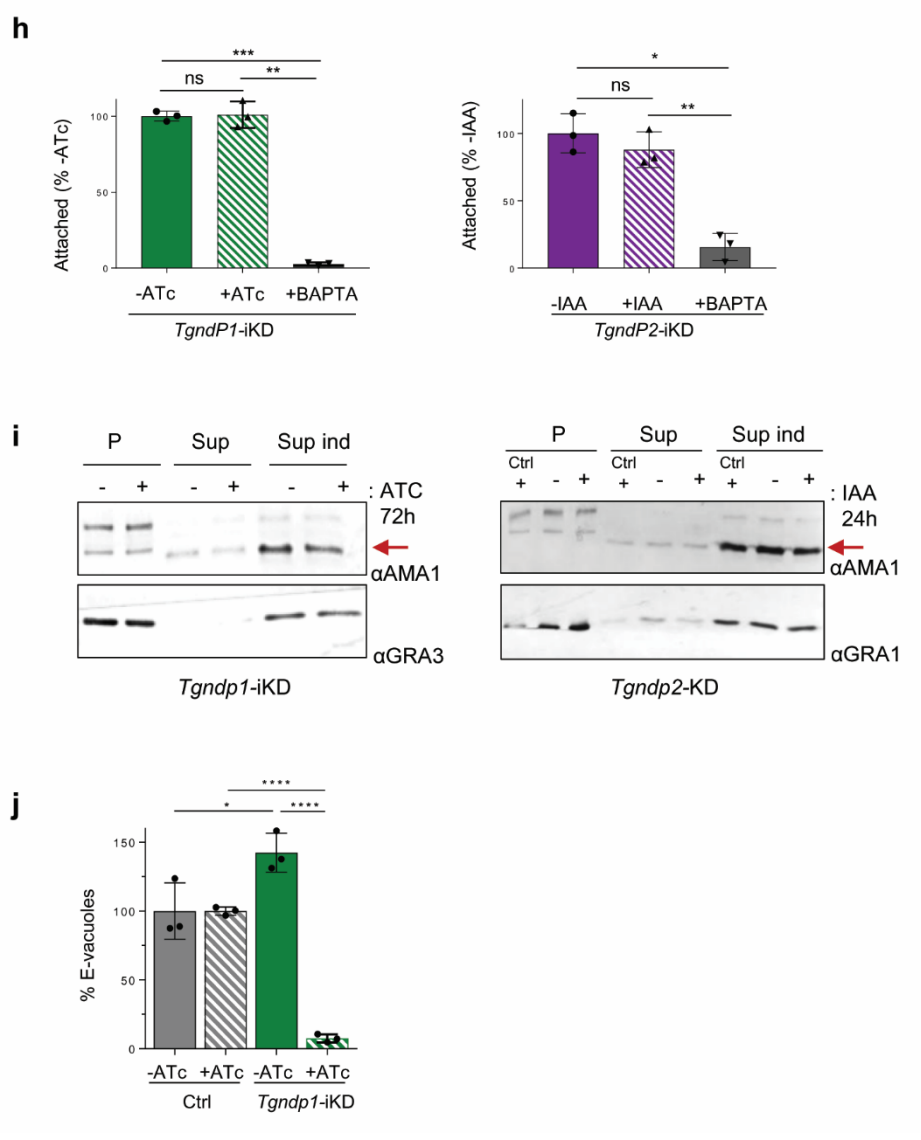
h
***
ns
**
Attached (% -ATc)
100
50
0
-ATc
+ATc
+BAPTA
TgndP1-iKD
*
ns
**
Attached (% -IAA)
100
50
0
-IAA
+IAA
+BAPTA
TgndP2-iKD
i
P
Sup
Sup ind
- + - + - +
: ATC
72h
αAMA1
αGRA3
Tgndp1-iKD
P
Sup
Sup ind
Ctrl
Ctrl
Ctrl
+ - + + - + + - +
: IAA
24h
αAMA1
αGRA1
Tgndp2-KD
j
****
*
****
% E-vacuoles
150
100
50
0
-ATc +ATc -ATc +ATc
Ctrl
Tgndp1-iKD

152

Extended Data Fig. 8 | Mucocyst biogenesis and positioning is not affected in *Tt*Δ*ndp1* and *Tt*Δ*ndp2*.

a, Generation of *Ttndp1* and *Ttndp2* knockout strains in *T. thermophila* Cu428. **b**, cDNA from *TtΔndp1* (clones 4 and 9) or *TtΔndp2* (Clones 1 and 5) were PCR amplified with primers P13/P14 and P21/P22 respectively, to assay the presence of the corresponding transcripts in the knockout strain. To confirm that equal amounts of cDNA were being amplified, reactions with primers specific for β-tubulin 1 were run in parallel (loading control). **c**, Immunoblot showing proGrl1p processing in wild-type and mutant strains (clones 4 and 9 for *TtΔndp1*; clones 1 and 5 for *TtΔndp2*). **d**, Confocal cross (top) and transverse (bottom) sections, with paired differential interference contrast (DIC) images, of *Tt*Δ*ndp1* (clone 9) and *Tt*Δ*ndp2* (clone 5). Cells were immunostained with mAbs 5E9, which recognize the mucocyst protein Grl3p. The wild-type pattern of the docked mucocysts is maintained in *Tt*Δ*ndp1* and *Tt*Δ*ndp2* clones. Scale bar = 10μm.

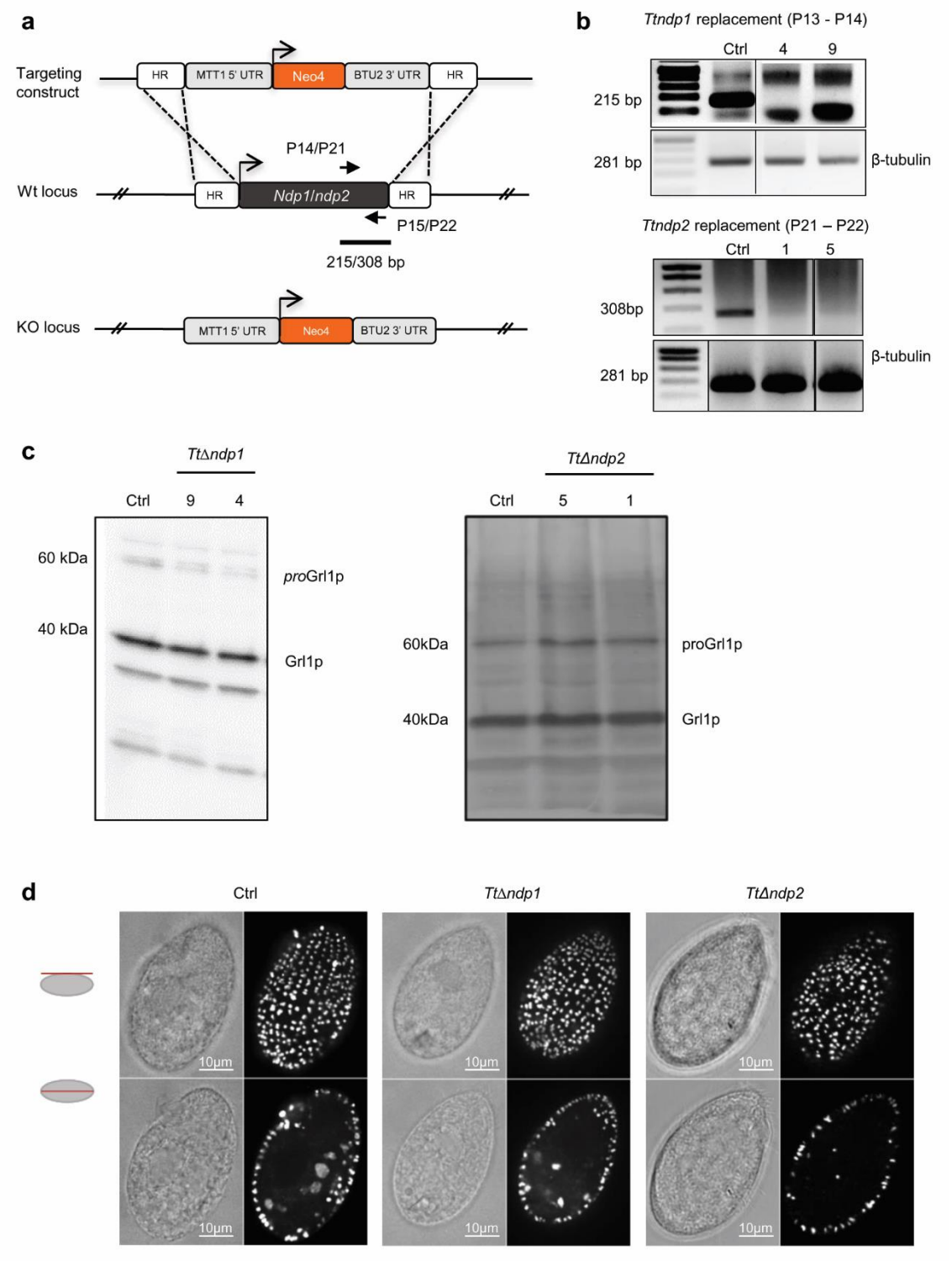
a
Targeting construct
HR
MTT1 5' UTR
Neo4
BTU2 3' UTR
HR
P14/P21
Wt locus
HR
Ndp1/ndp2
HR
P15/P22
215/308 bp
KO locus
MTT1 5' UTR
Neo4
BTU2 3' UTR
b
Ttndp1 replacement (P13 - P14)
Ctrl 4 9
215 bp
281 bp
β-tubulin
Ttndp2 replacement (P21 – P22)
Ctrl 1 5
308bp
281 bp
β-tubulin
c
TtΔndp1
Ctrl 9 4
60 kDa
40 kDa
proGrl1p
Grl1p
TtΔndp2
Ctrl 5 1
60kDa
40kDa
proGrl1p
Grl1p
d
Ctrl
TtΔndp1
TtΔndp2
10µm

166

167

Extended Data Fig. 9 | Cryo-ET of rhoptry secretion system

Four examples (a-d) from cryo-ET imaging of apical ends of the rhoptry secretion system. (i) vertical tomogram slices show the arrangement of the rhoptry (orange), tip density (cyan), apical vesicle (AV; magenta), rosette (dark blue) and the plasma membrane (PM; light blue). Original images (right) are annotated with color overlays (left). (ii) Magnified image of the boxed region in (i) showing the side view of the rosette. (iii) Top view of the rosette from a horizontal tomogram section through it and perpendicular to the plane in (ii) showing an 8-fold rotational symmetry. All measurements are made in 3D. Panel (a) shows images from the unfiltered version of the tomogram that is shown in Fig. 4a-c. In each of the four examples, images in (ii) and (iii) are from the same cell. Scale bars: 50 nm.

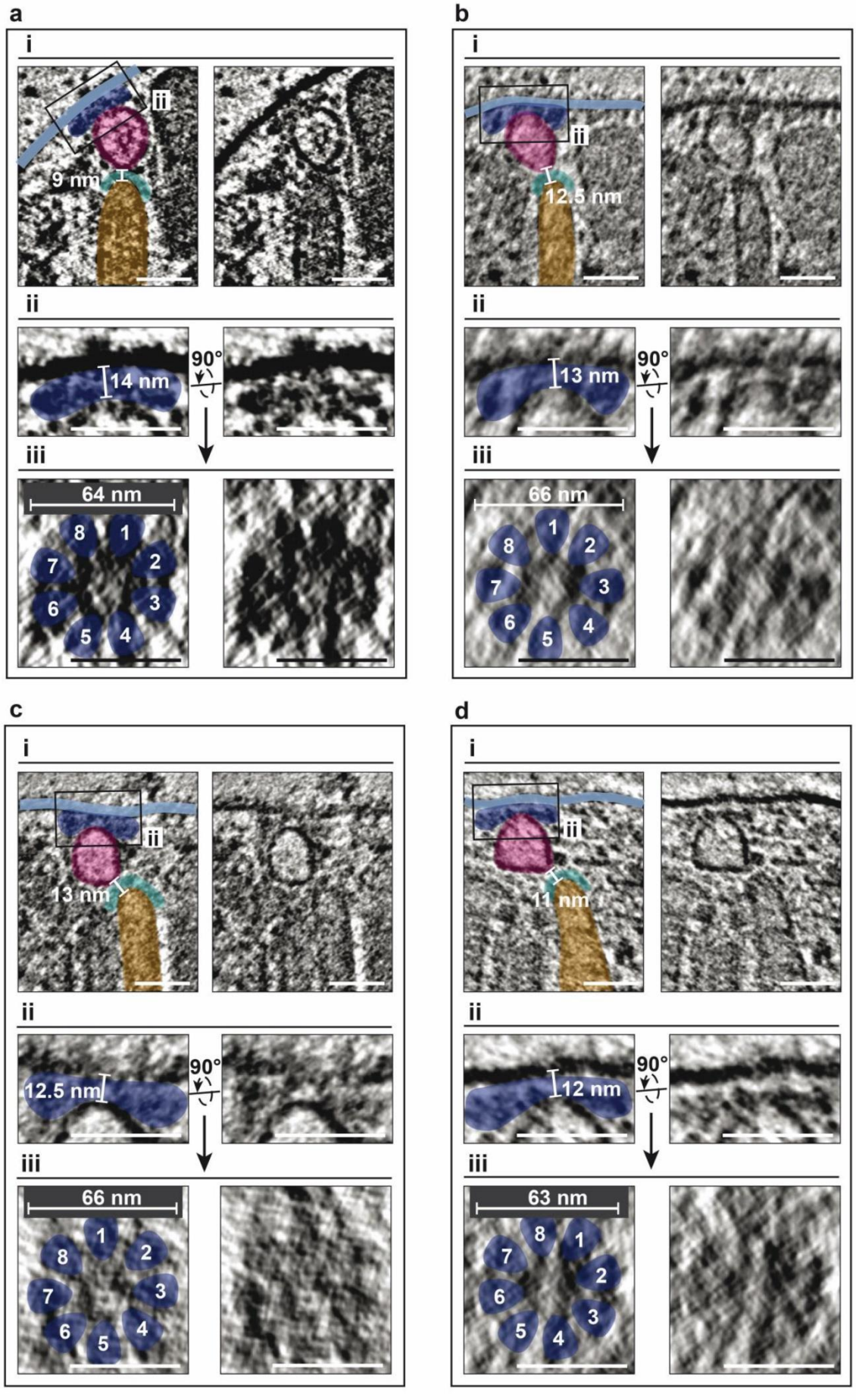
a
i
ii
9 nm
ii
14 nm
90°
iii
64 nm
8
1
7
2
6
3
5
4
b
i
ii
12.5 nm
ii
13 nm
90°
iii
66 nm
1
8
2
7
3
6
4
5
c
i
ii
13 nm
ii
12.5 nm
90°
iii
66 nm
1
8
2
7
3
6
4
5
d
i
ii
11 nm
ii
12 nm
90°
iii
63 nm
8
1
7
2
6
3
5
4

178

Extended Data Fig. 10 | Apical area of a *Sarcocystis tenella* cystozoite.

Similarly to what was observed in literature and experimentally in *T. gondii*, cystozoites of *S. tenella* display an apical vesicle in between the apical tip of the rhoptry neck and the plasma membrane, at the site of exocytosis. PCR = posterior preconoidal ring; co = conoid; Rh = rhoptry neck; m = micronemes; AV = apical vesicle. Bar is 0.2 µm.

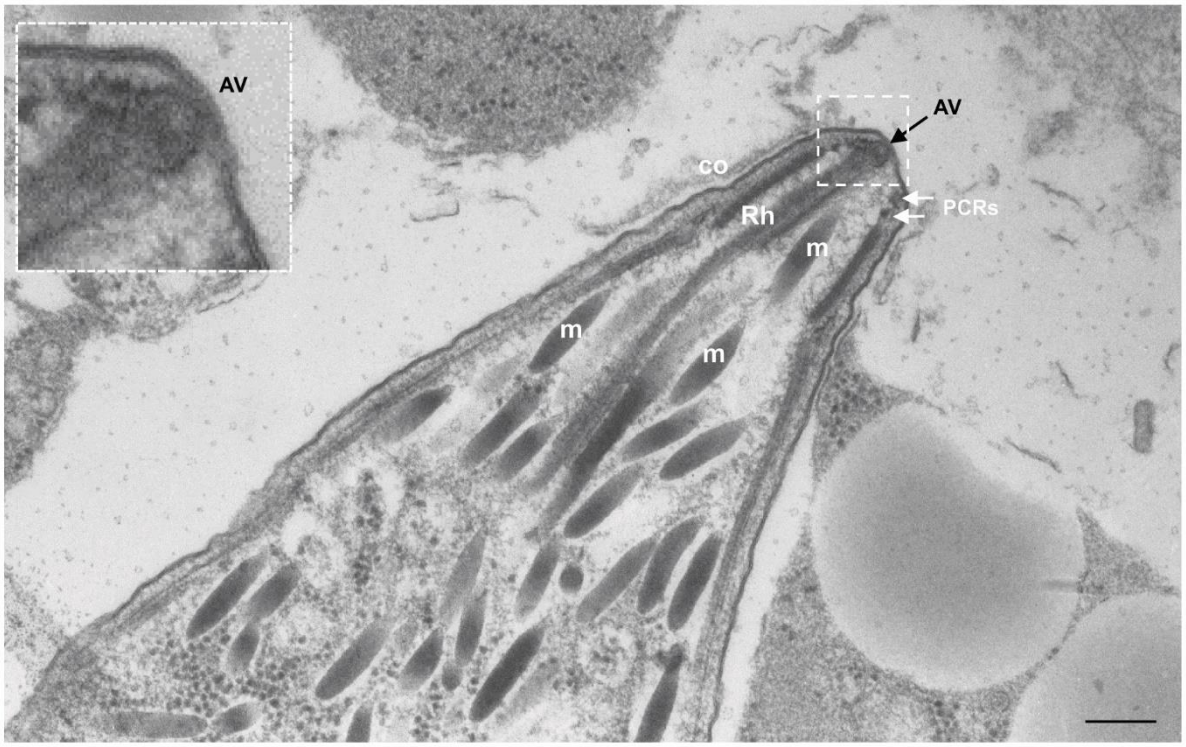

Extended Data Fig. 11 | Unedited full-length gels/blots used in main figures and Extended Figures

Fig. 1e

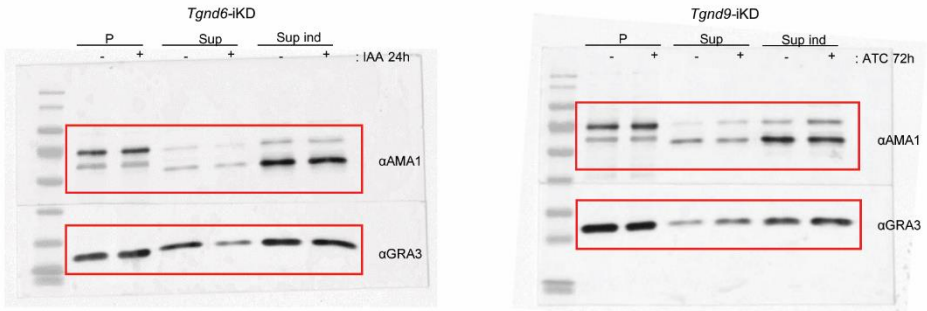

Extended Data Fig. 2b

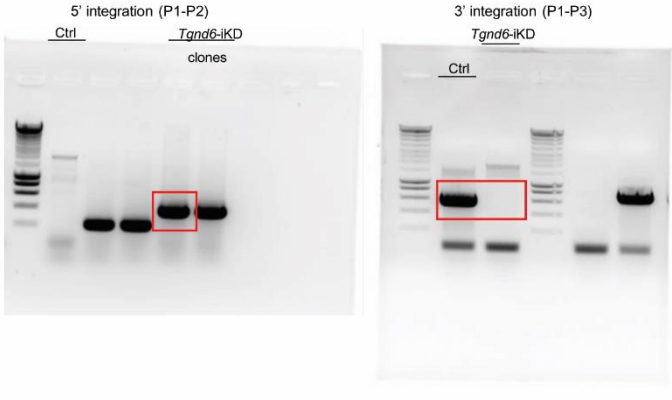

Extended Data Fig. 2d

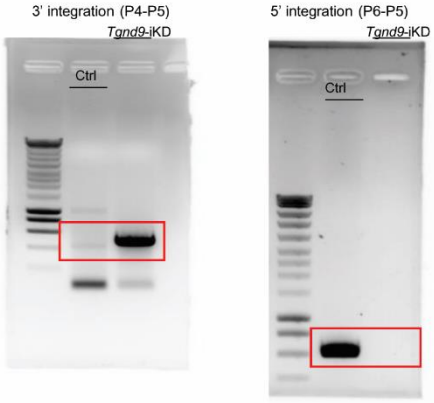

Extended Data Fig. 2e

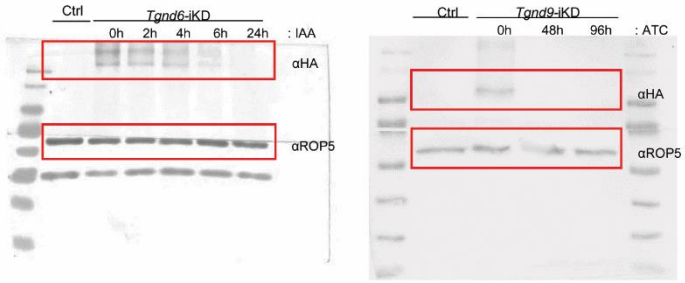

Extended Data Fig. 2g

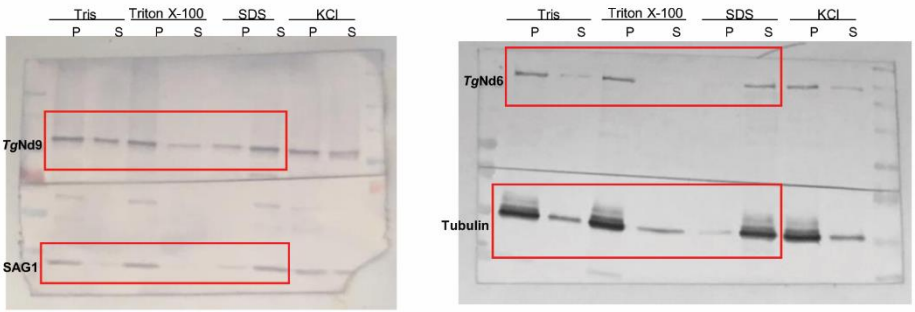

188

Extended Data Fig. 5b

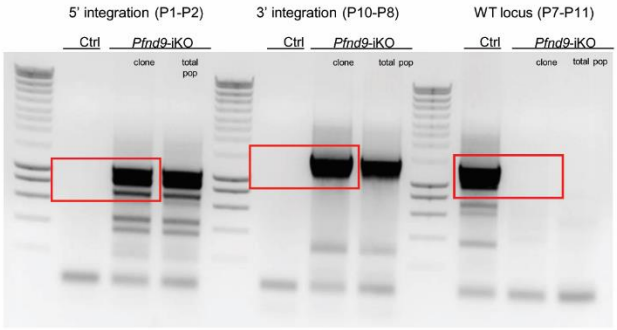

Extended Data Fig. 5c

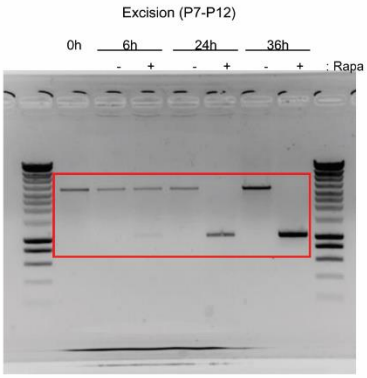

Extended Data Fig. 5d

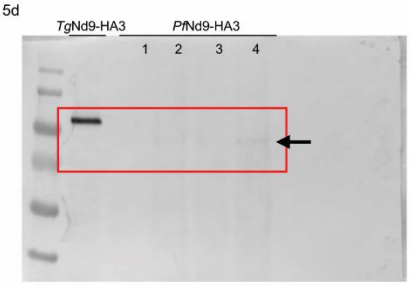

1: *rings*

2: *young trophozoites*

3: *young trophozoites*

4: *late trophozoites/schizonts*

Extended Data Fig. 6b

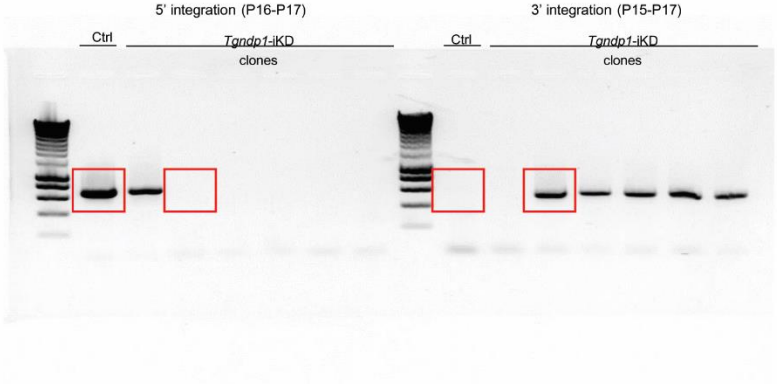

Extended Data Fig. 6d

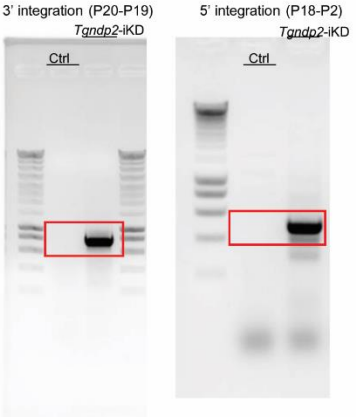

189

Extended Data Fig. 6e

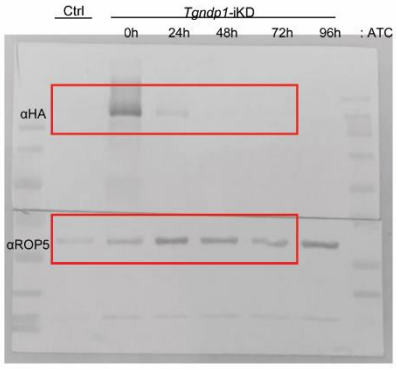

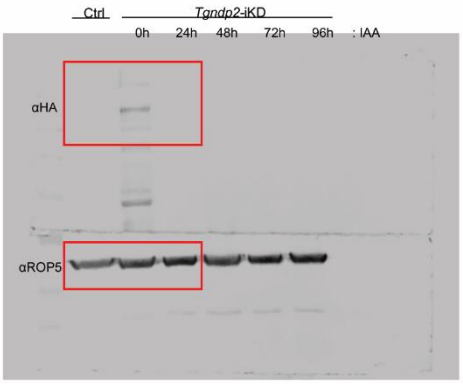

Extended Data Fig. 7i

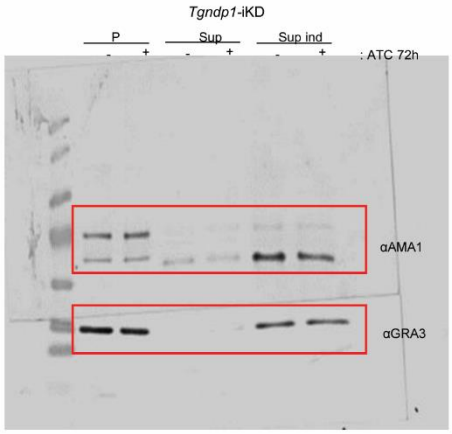

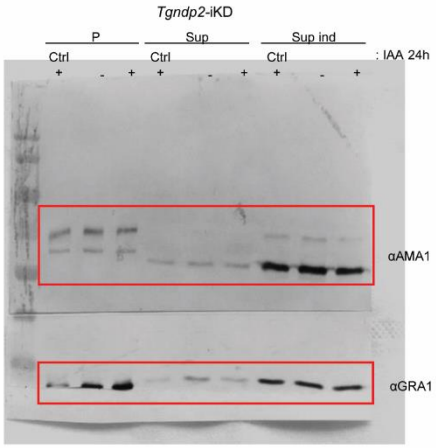

Extended Data Fig. 8b

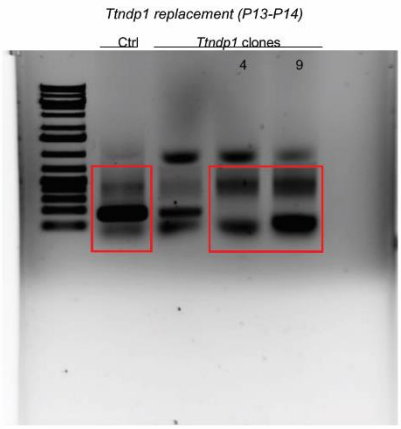

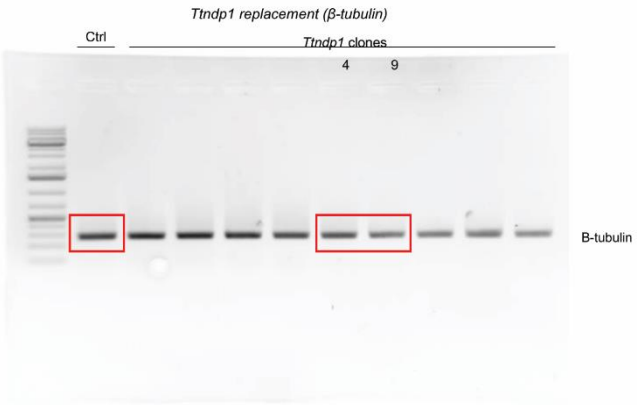

190

Extended Data Fig. 8b

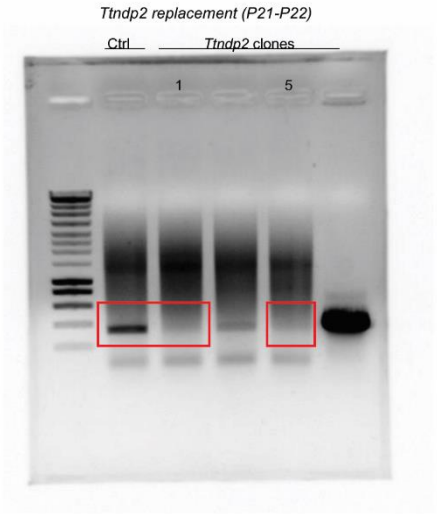

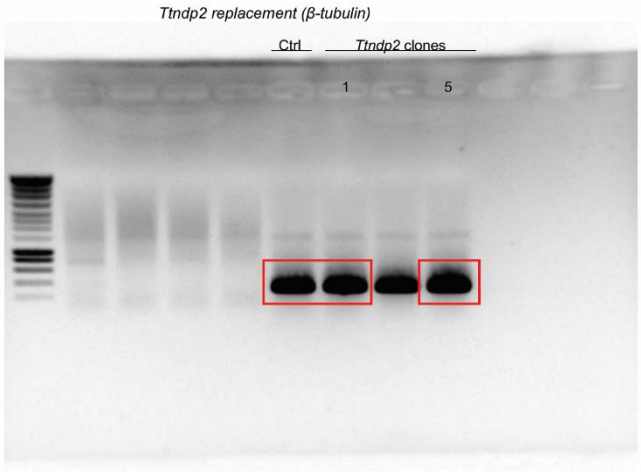

Extended Data Fig. 8c

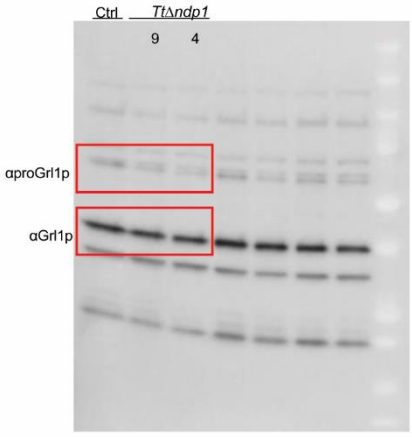

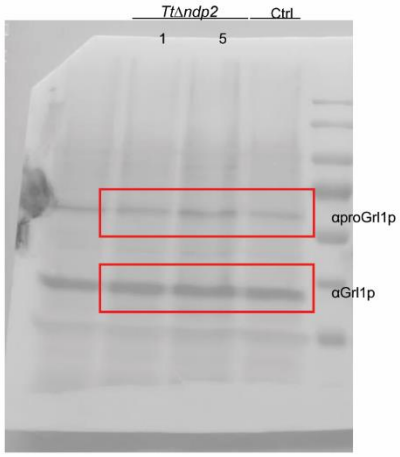

191

Supplementary Table 1 | Putative gene orthologues found in *Toxoplasma gondii* and *Plasmodium falciparum* using *Paramecium* protein sequences

	Putative genes orthologues found in *T. gondii* and *P. falciparum* using *Paramecium* proteins sequences	
Paramecium Nd proteins (UniProt ID)	*T. gondii*	*P. falciparum*
nd2[2] (Q8T314)	no clear ortholog	no clear ortholog
nd22[2] (Q7Z103)	no clear ortholog	no clear ortholog
nd6[3] (Q7Z102)	TGGT1_248640	PF3D7_0508500
nd7[4] (P90641)	No ortholog found	No ortholog found
nd9[5] (Q9GRI1)	TGGT1_249730	PF3D7_1232700
nd169[2] (Q70G70)	No ortholog found	No ortholog found

Supplementary text

None of the Nd factors are transmembrane proteins and thereby cannot be considered as candidates for IMPs of the rosette. However, our cryo-ET tomography revealed that an eight-fold symmetric structure extends under the parasite plasma membrane, suggesting that the IMPs of the rosette are part of a more complex secretion apparatus. Nd6, which is detected at the site of exocytosis (Fig. 1c), is therefore a prime candidate of this apparatus. NdP2, also visible at the apex (Fig. 3b), might be another constituent of the secretion machinery. Although we did not see accumulation of Nd9 and NdP1 at the apex, we cannot exclude that they might be present at concentrations below the detection limit of light microscopy. Conditional depletion of *Tg*Nd6 reduces rhoptry secretion but does not affect rosette assembly, in contrast with the *Paramecium* mutant where the absence of *Pt*Nd6 disrupts rosette formation[2]. The difference could be explained by technical limitations, due to the mutagenesis knockdown strategy for *Toxoplasma*, which might lead to incomplete protein depletion, as opposed to a complete removal of the gene in *Paramecium*[3]. Remarkably, since *Tg*ND6 is important for rhoptry secretion (fig. 1f), it supports a more direct role in the fusion event, possibly in the activation of a GTPase through its GEF domain. The situation for the other mutants is different. Indeed, depletion of the other Nd proteins compromises both rhoptry secretion and rosette formation, which suggests two possible scenarios: 1—they are key players of the fusion process, which together with Nd6 allows exquisite regulation of rhoptry release, or, 2—they are not responsible for the exocytosis event per se, but rather involved in the signaling pathway leading to the assembly of the rhoptry secretion machinery, a process which could be spatially and temporally regulated. The role of the Nds in controlling the fusion step, proposed in the first scenario, might rely on the correct assembly of Nd6, Nd9, NdP1 and NdP2 as a complex—together with the GTPase and the calcium-binding protein Ferlin 2, which were co-immunoprecipitated with Nd proteins (Fig. 3a). In

this case, all Nd proteins are part of the final secretion complex that controls membrane fusion in response to external stimulus. The correct assembly of such complex might be necessary to maintain the secretory machinery in a 'clamped' state that would prevent membrane mixing until an external signal prompt the fusion event. In the second scenario, without being part of the rhoptry secretion machinery, the cytosolic Nd9 and/or NdP1 would transiently interact with Nd6—which is associated with the apical vesicle—to trigger the assembly of the rosette at the center of the apex. These two scenarios are not mutually exclusive and calcium signaling and nucleotide binding/hydrolysis could be equally important for both.

The number of rhoptries varies between apicomplexan species. For instance, *Cryptosporidium* has one, the merozoites of *P. falciparum* two that fuse their necks at the time of invasion[4,5], while *T. gondii* has several (around twelve)[6]. Only one or two of these undergoes secretion during *T. gondii i*nvasion[7]. Interestingly, *Toxoplasma* also injects rhoptry proteins into cells that they do not invade[8] in order to deliver rhoptry effectors into the host and control the host immune response[9]. Since there is only a single rosette per parasite connected with a single AV at a fixed position at the apex of the cell, each burst of rhoptry secretion likely requires the building of a new rhoptry secretion apparatus. Notably, *Toxoplasma* possesses multiple vesicles, aligned from the apical tip through the conoid[10,11] (seen in figure 4g). It is tempting to speculate that these vesicles are used to dock rhoptries and to assemble rosettes involved in successive rhoptry exocytosis events. Remarkably, the alignment of similar vesicles was also observed in other organisms that possess several rhoptries[12,13].

Supplementary Table 2 | Mass spectrometry results of Nd9 Immunoprecipitation.

Supplemantary Table 3 | Mass spectrometry results of NdP1 Immunoprecipitation.

Supplemental Table 4 | List of primers used.

Extended Data 1 | Amino acid sequence alignments used to construct phylogenetic analysis

Supplementary Methods

Amino acid sequence alignments and phylogenetic analyses.

Sequences used in this study have been obtained from EuPathDB[14], NCBI and Dinoflagellata genomic database[15]. Multiple alignments of Nds protein amino acid sequences were computed using MAFFT[16] and cured using Noisy[17].

The alignments used for the phylogenetic analysis is presented in Supplementary Data 1-3. Phylogenetic analyses have been performed using PhyML-SMS on NGPhylogeny.fr[18]. Minimum of SH-like aLRT was used with LG[19,20] model of amino acids substitution and visualized using FigTree.

Cell and parasite culture

T. gondii tachyzoites RH strain (type I) deleted for *ku80* gene (*Δku80*)[21], and expressing the transactivator TATi (*Δku80-TATi*)[22] were routinely grown in human foreskin fibroblasts (HFFs) (ATCC, CRL 1634) monolayers, or Vero cells (ATCC, CCL 81) in Dulbecco's modified Eagle's medium (GIBCO) supplemented with 5% fetal calf serum, 2mM glutamine and 25µg/ml gentamicin (37°C, 5% CO2). For auxin-induced degradation, we used a *RHΔKu80* Tir1-expressing line (B. Striepen's lab). The hypoxanthine-xanthine-guanine phosphoribosyl transferase (HXGPRT), the uracil phosphoribosyl transferase (UPRT), chloramphenicol (CHL) and dihydrofolate reductase thymidylate synthase (DHFR-TS) selection genes were used as positive and/or negative selectable markers as previously described. Stable floxed DsRed-expressing mouse fibroblast cell line 10T1/2 was used as Cre-reporter cells for rhoptry secretion experiments with SeCrEt (strain secreted Cre, epitope-tagged) parasites[23].

P. falciparum 3D7 stable DiCre-expressing parasite line - *p230p*[24] - was used for all experiments. The asexual stages were cultured at 37°C in an atmosphere of 5% CO_2, 5% O_2 and 90% NO_2 with RBCs at 5% haematocrit in complete medium: RPMI 1640 medium (Gibco) supplemented with gentamycin at 20 µg/ml, 5% human serum and 2.5 mg/mL Albumax II® (Gibco). The RBCs were provided by the French Blood bank (Etablissement Français du Sang, Pyrénées Méditerranée, France). Parasite cultures were kept highly synchronized by combining Percoll purification of schizonts and sorbitol lysis treatments[25]. Highly synchronized cultures were used to characterize *Pf*Nd9 by immunoblots, growth assays, time-lapse microscopy (egress assays) and immunofluorescence (rhoptry and microneme secretion assays). In order to assess *Pf*Nd9 role in *P. falciparum* asexual stages, 10 nM rapamycin was added to early ring stage parasites and maintained for 24 hours to completely excise the floxed *Pfnd9* locus.

Parasite cloning strategies

All primers used in this study are listed in Supplementary Table 4.

Genomic DNA was isolated using Wizard SV genomic DNA purification system (Promega). All cloning PCR amplifications were performed with the KOD HiFi polymerase (Merk), otherwise PCR screenings were performed with GoTaq DNA Polymerase (Promega). RNA was purified using RNeasy Mini Kit (Qiagen). Total cDNA was generated by RT–PCR using High-Capacity cDNA Reverse Transcription Kit (Applied Biosystems) according to the manufacturer's protocol.

Tgnd6 (TGGT1_248640), *Tgnd9* (TGGT1_249730), *Tgndp1* (TGGT1_222660) and *Tgndp2* (TGGT1_316730) have been tagged with a triple hemagglutinin (HA_3) in the *Δku80-TATi* line by CRISPR/Cas9. Briefly, RNA guides (gRNA) were generated by annealing primers ML3129/ML3130, ML2958/ML2959, ML3040/ML3041 and ML3730/3731 respectively; the

annealed DNA fragments were cloned in the BsaI sites of vector pU6-Cas9 to obtain pU6-Cas9_*nd6*CtTag, pU6-Cas9_*nd9*CtTag, pU6-Cas9_*ndp1*CtTag and pU6-Cas9_*ndp2*CtTag. Donor DNA sequences containing the HA_3 tag and a generic 5' UTR, in addition to the chloramphenicol resistance gene (CAT) under the pTUB promoter were amplified from pLIC_3HA_CAT vector[21] using the primers ML2982/ML2983, ML2956/ML2962, ML3042/ML3043 and ML4331/ML4332, containing 30 bp homology arms specific for the 3′ end of *Tgnd6, Tgnd9, Tgndp1* and *Tgndp2* without the stop codon, and the 3'UTR downstream of the gene. Stable transformants were selected with chloramphenicol 20 µM and clones were isolated by limiting dilution. For each transfection, clones were screened by PCR for correct integration. For *Tgnd6* localization studies, Centrin 2 (CEN2) was tagged with a double Ty peptide in the *Tgnd6*-HA3 background line using the same strategy as previously described for HA_3 tagged lines. The gRNA plasmid (pU6-Cas9_CEN2CtTag) was a gift from Soldati's lab. The donor DNA sequence containing also a dihydrofolate reductase thymidylate synthase resistance gene (DHFR-TS) was amplified from pLinker-2xTy-DHFR plasmid (Soldati´s lab) using the primers ML4583/ML4584. For *Tg*Nd6 and *Ring-1* (RNG1) co-localization studies, RNG1 was transiently expressed with a green fluorescent protein (GFP) by transfecting a *RNG1-GFP* plasmid (gift from Waller´s lab).

Conditional knockdowns of *Tgnd9* and *Tgndp1* genes were generated in the tagged background lines *Tgnd9*-HA_3 (*Tgnd9*-iKD) and *Tgndp1*-HA_3 (*Tgndp1*-iKD). For this purpose, we designed a Tet-OFF system using CRISPR/Cas9. Plasmids pU6-Cas9_*nd9*NtTetO and pU6-Cas9_*ndp1*NtTetO were generated using primers ML2965/ML2966 and primers ML3173/ML3174 to induce a double-stranded break at the 5' of the GOI. PCR fragments encoding a selectable DHFR resistance cassette and the TetO7S1 promoter were amplified from the DHFR-TetO7-SAG4 plasmid with primers ML2963/ML2964 and ML3121/ML3122 (harbouring 30 bp homology arms specific for the 5' UTR upstream the GOI, and the first 30

bp of the genes (including the START codon). Stable transformants were selected with 1 µM pyrimethamine and clones were isolated by limiting dilution. For each transfection, clones were screened by PCR for correct integration.

Auxin-inducible degradation and tagging of *Tgnd6* (*Tgnd6*-iKD) and *Tgndp2* (*Tgndp2*-iKD) were obtained with one single transfection fusing AID, the HA_3 tag, and the DHFR cassette in frame at the end of *Tgnd* gene, before the STOP codon, in the *ΔKu80-Tir1* parasite line. Template DNAs have been amplified from the vector pLIC.tAID.3xHA.DHFR.Lox using the KOD DNA polymerase (Novagen, Merck) and primers ML3131/ML3132 (*Tgnd6*) and ML3734/ML3735 (*Tgndp2*). Previously generated pU6-Cas9_*nd6*CtTag and pU6-Cas9_*ndp2*CtTag plasmids were used to introduce a double-stranded break at the 3′ of *Tgnd6* and *Tgndp2*, respectively. Stable transformants were selected with 1 µM pyrimethamine and clones were isolated by limiting dilution. For each transfection, clones were screened by PCR for correct integration.

Secreted Cre epitope-tagged (SeCreEt) parasite lines were obtained by inserting the hemagglutinin (HA)-tagged toxofilin (rhoptry protein)-Cre recombinase into the uracil phosphoribosyltransferase (UPRT) gene for *Tgnd9*-iKD (*Tgnd9*-iKD_SeCrEtUPRT) and *Tgndp1*-iKD (*Tgndp1*-iKD_SeCrEtUPRT), or into the hypoxanthine-xanthine-guanine phosphribosyl transferase (HXGPRT) gene for *Tgnd6*-iKD (*Tgnd6*-iKD_SeCrEtHXGPRT) and *Tgndp2*-iKD (*Tgndp2*-iKD_SeCrEtHXGPRT), using CRISPR/Cas9. Specific single guides RNA (sgRNAs) were generated to cut the 5' ML3445/ML3446 and 3' ML2087/ML2088 of the UPRT locus, and to disrupt the HXGPRT locus ML4275/ML4276. Amplification of template DNA was done with primers ML3522/ML3523 (UPRT) and with primers ML3923/ML3959 (HXGPRT) flanked by 30 bp homology arms. Stable transformants were negatively selected for loss of the UPRT locus with 5 µM pro-drug 5′-fluo-2′-deoxyuridine (FUDR)[26], and for HXGPRT locus substitution with 200 µg/ml 6-Thioxanthine

(6-TX)[27]. Clones were isolated by limiting dilution. For each transfection, clones were screened by PCR for correct integration.

To construct a conditional deletion vector for *Pfnd9* (PF3D7_1232700), two PCR products corresponding to 684 bp of the *pfnd9* 5'UTR (primers ML3257/ML3258) and to 2.4 kb of *Pfnd9* exon 1 (primers ML3259/ML3298), together with LoxPint[28] and recodonized exons 2-18 of *Pfnd9,* were assembled by *In-Fusion HD* (Clontech 638918) into the plasmid pFloxed_PfRASP2-HA_3[29]. This vector was previously digested with BamHI and BsiWI to remove the 5'UTR and the floxed *Pfrasp2* sequence, but conserved the generic 3'UTR (PbDT3'). The 5'UTR (=homology region 1) was amplified from gDNA and the floxed *Pfnd9* CDS was ordered as a synthetic gene (GeneWiz, codon optimisation for *S. frugiperda*). The synthetic gene contained the first natural exon of *Pfnd9,* a LoxPint replacing the first endogenous intron as well as the recodonized exons 2-18. The homology region 2 of the final donor vector was assembled by *In-Fusion HD* by amplifying 550 bp of *Pfnd9* 3'UTR from gDNA (primers ML3702/ML3703) and cloned at the HpaI/NotI sites. This assembly resulted in a floxed recodonized *Pfnd9* cDNA sequence in addition to a triple HA tag (donor plasmid). Before transfection, this donor plasmid was linearized with XbaI. The resulting parasite line was designated as *Pfnd9*-iKO. A sgRNA targeting exon 14 of *Pfnd9* was selected using the Eukaryotic Pathogen CRISPR gRNA Design Tool[30]. The sgRNA sequence was cloned in the pDC2-Cas9-hDHFRyFCU plasmid[28] using the annealed primers ML3962/ML3963, and named pDC2-Cas9-*Pfnd9*. Transgenic parasites were grown under agitation (200 rpm) and selected by 2.5 nM WR99210 for 10 days with daily media changes. The growth of resistant parasites was monitored by visualizing Giemsa-stained blood smears by light microscopy. Viable parasites were screened by PCR for floxed *Pfnd9* genome integration, previous to cloning by limiting dilution. 5' and 3' integration of floxed *Pfnd9* into the genome was detected by PCR using primers ML3784/ML3786 and ML3785/ML3787, respectively.

Absence of wt locus was verified using primers ML3784/ML3788. DiCre recombinase-mediated excision of the floxed *Pfnd9* locus upon rapamycin treatment, was confirmed by PCR with primers ML3784/ML3789.

Parasite transfections

For *T. gondii*, $20x10^6$ tachyzoites were transfected by electroporation at 2.02 kV, 50 Ω, 25 µF in a Electro Cell Manipulator 630 (BTX) with 5 µg of PCR products obtained with the KOD polymerase in addition to 20 µg of CRISPR/Cas9 plasmid, as previously described [31].
P. falciparum parasites were transfected by electroporating 5%-10% ring-stage parasites[32]. 30 µg of the circular plasmid *(*pDC2-Cas9_gRNA *Pfnd9*) were co-transfected with 60 µg of the linearized donor plasmid into *p230p* line, generating *Pfnd9*-iKO parasite line.

Proteins solubility and parasite immunoblots

Equal amount ($6x10^6$) of freshly egressed *T. gondii* tachyzoites were harvested, washed in PBS and resuspended directly in SDS sample buffer. SDS-PAGE and Western blotting were done as previously described[33]. Detergent extraction was adapted from Lentini et al.[34].

***T. gondii* plaque assays**

HFF monolayers grown in 24-well plates were infected with parasites (~100) from the background lines (*Δku80-TATi* or *ΔKu80-Tir1*) or the iKD lines (*Tgnd9*-iKD, *Tgndp1*-iKD and *Tgnd6*-iKD, *Tgndp1*-iKD) with or without (±) ATc or IAA, respectively. After 7 days, HFF monolayers were fixed with 4% paraformaldehyde (PFA)-PBS and stained with Giemsa. Images were obtained with an Olympus MVX10 macro zoom microscope equipped with a

Zeiss MRM2 Camera. Plaque area measurements were performed with Axiovision (Zeiss) software. Images were taken at the MRI facility at the University of Montpellier.

T. gondii intracellular growth assay

HFF monolayers grown on coverslips in a 24-well plate were infected with $2x10^5$ freshly egressed parasites of the background lines (*Δku80-TATi* or *ΔKu80-Tir1*) or the iKD lines. *Tgnd9*-iKD and *Tgndp1*-iKD were pre-treated ± ATc 48h before infection. After 2 hours of incubation at 37°C, the remaining extracellular parasites were removed by washing the HFF cells five times with HBSS. Then, the infected cells were incubated for additional 22 hours at 37°C and fixed with 4% PFA in PBS. Intracellular parasites were stained by IFA using mouse mAb T4 1E5 anti-SAG1, and the number of parasites per vacuole was counted from 200 vacuoles per coverslip (n=3 coverslips). The replication assay was performed in triplicates.

T. gondii immunofluorescence-based induced egress assay

$1×10^5$ parasites were added to HFFs grown on coverslips in a 24-well plate and allowed to grow for ∼30 hrs. Parasites egress was stimulated with 3 μM A23187 for 8 min before samples were fixed and processed for IFA (anti-GRA3 antibodies). Egress events (GRA3 in the PV) were quantified by analysing 200 vacuoles per coverslip (n=3 coverslips). Graph shows one representative egress assay.

T. gondii conoid extrusion assay

Freshly egressed *T. gondii* tachyzoites (parental strains and iKD lines pre-treated 72 h ± ATc in the case of *Tgnd9*-iKD and *Tgndp1*-iKD and 24 h ± IAA in the case of *Tgnd6*-iKD and *Tgndp2*-iKD) were pelleted and re-suspended in 20mM HEPES containing 5mM $CaCl_2$ and 5 μM calcium ionophore A23187 to induce protrusion, or DMSO as control. Parasites were then

incubated for 8 min at 37°C on Poly-L-lysine coated coverslips and fixed for 30 min with 4% PFA. Protruded and non-protruded parasites were counted using the 63x magnification under Differential Interference Contrast (DIC) condition. The average number of protruded parasites was determined by counting 200 parasites for each condition in three independent experiments.

T. gondii gliding assay

$5x10^6$ freshly egressed parasites of the background lines (*Δku80-TATi* or *ΔKu80-Tir1*) or the iKD lines (*Tgnd9*-iKD, *Tgndp1*-iKD or *Tgnd6*-iKD, *Tgndp2*-iKD) pre-treated with or without ATc for 72h or IAA for 24h, respectively, were harvested and resuspended in 500 µL of Ringer's medium (155 mM NaCl, 3 mM KCl, 2 mM $CaCl_2$, 1 mM $MgCl_2$, 3 mM NaH_2PO_4, 10 mM HEPES, 10 mM glucose) containing 1 µM calcium ionophore A23187 (Calbiochem, EMD Chemicals, USA). Immediately, 100 µL of the parasite suspension was placed on poly-L-lysine coated slides and incubated at 37°C in a wet environment. After 15 minutes, unattached parasites were removed by washing with PBS, and IFA were performed on 4% PFA-fixed parasites, using mouse mAb T4 1E5 anti-SAG1 to visualize the trails of SAG1 formed by gliding.

Video microscopy and analysis of _T. gondii_ motility

Parasites of the background lines (*Δku80-TATi* or *ΔKu80-Tir1*) or the iKD lines (*Tgnd9*-iKD, *Tgndp1*-iKD or *Tgnd6*-iKD, *Tgndp2*-iKD) were treated with either ATC for 48h or IAA for 24h. Freshly egressed parasites were placed on gelatin-coated glass (µ-Slide 4 Well, IBIDI), settled via a small spin at 1.100rpm for 1 minute and then stimulated with BIPPO (5 µM). At least 3 videos of 60 seconds were recorded for each conditions. Time-lapse videos were taken by Nikon digital sight camera at 25 frames per second on a Nikon eclipse Ti inverted

463 microscope using a 63 x oil immersion objective. The whole apparatus was temperature-
464 controlled to maintain the samples at 37°C during the all duration of the acquisition. The type
465 of motility (helical, twirling and circular) were scored by the observers. Data presented the
466 values of at least 43 parasites for each strain from 3 to 4 independent movies. An average of
467 25 parasites was counted per video.
468
469 ***T. gondii* attachment assay**
470 HFFs grown on coverslips in a 24-well plate were fixed in 2% glutaraldehyde/PBS for 5 min
471 at 4°C. Cells were washed 3 times with cold PBS, then quenched with 100 mM Glycine for 2
472 min. Cells were washed in PBS before to infect each coverslip with 10 million of parasites in
473 300 µl of DMEM/5% FBS. As a negative control for microneme-dependent attachment,
474 parasites were treated with 20 µM BAPTA-AM (Sigma) for 20 min at 37°C before infection.
475 Parasites were allowed to attach for 20 min at 37°C, washed 2 times with DMEM/5% FBS,
476 and fixed with 4% PFA for 20 min. Following quenching with 100 mM glycine for 2 min,
477 cells were washed three times with PBS and attached parasites were stained by
478 immunofluorescence using 1:500 rabbit anti-SAG1 and 1:1000 goat anti-rabbit Alexa Fluor
479 488. Twenty random fields were counted per coverslip (n=3 coverslips).
480
481 **Ciliata culture conditions**
482 *T. thermophila* described as wild type in the text refers to CU428.1 (*Tetrahymena* Stock
483 Center, Cornell University, Ithaca, NY, USA). Cells were routinely grown at 30°C with
484 shaking at 99 rpm in SPP medium (2% proteose peptone. 0.2% dextrose, 0.1% yeast extract,
485 0.003% ferric EDTA) supplemented with 250 ug/ml penicillin G, 250 µg/ml streptomycin
486 sulfate, and 0.25 µg/ml amphotericin B fungizone, to medium density (1-3 x 105 cells/ml).

Culture densities were measured using a Z1 Coulter Counter (Beckman Coulter) or counted with a Neubauer chamber upon fixation with Acetic Acid and methanol.

Ciliata biolistic transformation

Tetrahymena transformants were generated and selected after biolistic transformation as previously described[35,36]. Transformants were serially transferred 6x/week in increasing concentrations of paromomycin and decreasing concentrations of $CdCl_2$ (up to 1-2 mg/ml of paromomycin and 0.1 μg/ml $CdCl_2$) for at least 5 weeks before further testing. At least three independent transformants were tested for each line.

Generation of *Tetrahymena* knockout strains

To obtain the *T. thermophila ndp1* (TTHERM_01287970) and *ndp2* (TTHERM_00498010) knockout strains the macronuclear (MAC) open reading frame (ORF) of gene was replaced with the paromomycin (Neo4) drug resistance[37] via homologous recombination with the linearized p*ndp1*MACKO-Neo4 or p*ndp2*MACKO-Neo4 vectors. Briefly, PCR was used to amplify 500-800 bp of the genomic regions upstream (5'UTR) and downstream (3'UTR) of the ORFs. The amplified fragments were subsequently cloned into SacI/PstI (5'UTR) and HindIII/XhoI (3'UTR) restriction sites, flanking the Neo4 cassette of the pNeo4 vector, by Quick Ligation (New England, Biolabs Inc.) to build p*ndp1*MACKO-Neo4, and cloned into SacI/PstI (for 5'UTR) and XhoI/KpnI (for 3'UTR) restriction sites, with the same strategy to build p*ndp2*MACKO-Neo4. The primers used to create these constructs are AT35/AT36, AT39/AT40 (p*ndp1*MACKO-Neo4) and AT21/AT22, AT23/AT24 (p*ndp2*MACKO-Neo4). The constructs were linearized by digestion with SacI and XhoI, and SacI and KpnI, respectively, and transformed into CU428.1 cells by biolistic transformation.

We assessed *Ttndp1* and *Ttndp2* disruption by RT-PCR. $3x10^5$ cells from overnight cultures were pelleted, washed once with 10mM Tris, pH 7.4, and total RNA was isolated using RNeasy Mini Kit (Qiagen, Valencia, CA). The cDNA synthesis, from 3 μg of total RNA, was performed using High-Capacity cDNA Reverse Transcription Kit (Applied Biosystems, Foster City, CA). The cDNA was PCR amplified with primers to assay the presence of *Ttndp1* and *Ttndp2* gene transcripts in the knockout strain, using primers AT41/AT42 (*Ttndp1*) and ML3887/ML3888 (*Ttndp2*). To confirm that equal amounts of cDNA were being amplified, reactions with primers AT55/AT56 specific for β-tubulin 1 (BTU1) were run in parallel.

Ciliata immunoblots

Protein samples were analysed by western blot as previously described[38]. Rabbit anti-Grl1p serum was diluted 1:2000 in 5% milk blocking solution. Proteins were visualized either with anti-rabbit IgG (whole molecule)-HPeroxidase (Sigma) secondary antibody diluted 1:20000, or with anti-rabbit IgG AP-conjugated secondary antibody (1:7500, S3731, Promega). Membranes were washed and incubated either with SuperSignal West Femto Maximum Sensitivity Substrate (Thermo Scientific), or with BCIP/NBT Color Development Substrate (Promega) to visualize protein signals.

Ciliata immunofluorescence microscopy

Wild-type and *Ttnd* knockout cells ($5x10^5$) were washed, fixed with 4% PFA for 30 min, and immunostained as previously described[39,40] Grl3p was visualized using mouse mAb 5E9 (1:10), followed by either Texas Red-conjugated goat anti-mouse antibody (1:100) (Life Technologies, Carlsbad, CA), or Alexa Fluor 488-conjugated anti-mouse antibody (1:250) (Molecular Probes), all in 1% BSA-PBS blocking solution. Immunostained cells were mounted with 30% glycerol-PBS, supplemented with Trolox (1:1000) to inhibit bleaching,

and imaged either on a Marianas Yokogawa type spinning disk inverted confocal microscope, 100X oil with NA=1.45 with Slidebook6 software (Zeiss, Intelligent Imaging Innovations), or on a Zeiss Axioimager Z2/Apo fluorescence microscope, 100X oil with NA=1.46 with Zen software (Zeiss, Intelligent Imaging Innovations). Z-stack images (10-16 stacks along the z-axis at 0.5 μm intervals) were colored, de-noised and adjusted in brightness/contrast with the program Fiji[41]. Images shown are single slices for clarity.

Statistical analyses

All results are presented as mean values with standard deviations shown as error bars. No statistical tests were used to predetermine sample size. Two-tailed Student's *t*-tests was used appropriately to determine statistical significance for invasion, replication, egress, attachment, microneme and rhoptry secretion assays. A *p*-value of 0.05 was considered significant.

Reagents

Cytochalasin D (Sigma C8273) was prepared at 1 mM in DMSO and used at 1 μM final concentration. ATc (Fluka 37919) was prepared in 1 mg/ml in ethanol and used at 1 μg/ml final. Indolacetic acid (IAA) (ChemCruz sc-215171) stock was prepared at 1 M in methanol and used at 1 mM final concentration. Propranolol (Sigma P0884) was prepared at 100 mM in DMSO and used at 500 μM final concentration. A23187 stocks prepared at 2 mM and used at 3 μM final concentration. Compound 2 (4-[7-[(dimethylamino)methyl]-2-(4-fluorphenyl)imidazo[1,2-α]pyridine-3-yl]pyrimidin-2-amine (C2) was a kind gift from Dr. O. Billker (Sanger Institute, Cambridge, UK), stock solution was prepared in DMSO (3 mM) stored at -20°C, and used at final concentration of 1 μM. Rapamycin (rapa) and E64 were obtained from Sigma (catalogue numbers R0395 and E3132); stock solutions (100 μM for rapa and 50 mM E64) were prepared in DMSO, stored at −20°C, and used at final

concentrations of 10 nM (rapa) and 50 μM (E64). The antifolate drug WR99210 was from Jacobus Pharmaceuticals (New Jersey, USA) and used at 2.5 nM final concentration.

Antibodies

The antibodies used and their dilution for Western blot (WB) and immunofluorescence (IFA) were as follows:

-mouse mAb T4 1E5 anti-*Toxoplasma* SAG1, 1:2000 (IFA and WB)[42]

-rabbit anti-*Toxoplasma* ROP1, 1:3000 (IFA)[43]

-rabbit anti- *Toxoplasma* ARO, 1:500 (IFA)[44]

-rabbit anti-*Toxoplasma* AMA1, 1:5000 (WB)[45]

-mouse mAb CCL2 anti-*Toxoplasma* AMA1, 1:100 (IFA)[46]

-mouse mAb T5 3E2 anti-*Toxoplasma* ROP5, 1:200 (IFA)[47]

-rabbit anti-*Toxoplasma* GAP45, 1:9000 (IFA)[48]

-mouse anti-*Toxoplasma* GRA3 T6 2H11 1D1 hybridoma, 1: 100 (IFA)[49]

-mouse T34A11 anti-*Toxoplasma* MIC2, 1/200 (IFA)[50]

-mouse anti-*Plasmodium* MSP1 1:1000 (IFA)[51]

-rabbit anti-*P. falciparum* AMA1, 1:1000 (IFA)[52]

-mouse anti-*P. falciparum* RAP2, 1:500 (IFA)[53]

-mouse hybridoma supernatant anti-c Myc 9E10, 1:10 (IFA)

-mouse mAb 5E9 anti- *Tetrahymena* Grl3p, 1:10 (IFA)[54]

-rat anti-HA 3F10 (Roche), 1:500-1:1000 (IFA and WB)

-mouse mAb anti-c-Myc 9E10 1:250 (Sigma)

-mouse anti-α-tubulin (clone B-5-1-2, Sigma–Aldrich)

585 For IFA studies, the secondary antibodies used were Texas-red, Alexa Fluor 488 and 594-
586 conjugated antibodies against mouse, rat or rabbit IgG (highly cross-adsorbed) diluted as
587 recommended by the manufacturer (Molecular Probes). For immunoblots, the secondary rat,
588 mouse or rabbit antibodies used were coupled to alkaline phosphatase (Promega).
589
590 **Supplementary References**

591 1. Hakansson, S., Morisaki, H., Heuser, J. & Sibley, L. D. Time-lapse video microscopy
592 of gliding motility in *Toxoplasma gondii* reveals a novel, biphasic mechanism of cell
593 locomotion. *Mol Biol Cell* **10**, 3539–47 (1999).
594 2. Lefort-Tran, M., Aufderheide, K., Pouphile, M., Rossignol, M. & Beisson, J. Control
595 of exocytotic processes: cytological and physiological studies of trichocyst mutants in
596 *Paramecium tetraurelia*. *J Cell Biol* **88**, 301–11 (1981).
597 3. Gogendeau, D., Keller, A. M., Yanagi, A., Cohen, J. & Koll, F. Nd6p, a novel protein
598 with RCC1-like domains involved in exocytosis in *Paramecium tetraurelia*. *Eukaryot*
599 *Cell* **4**, 2129–39 (2005).
600 4. Aikawa, M., Miller, L. H., Johnson, J. & Rabbege, J. Erythrocyte entry by malarial
601 parasites. A moving junction between erythrocyte and parasite. *J Cell Biol* **77**, 72–82
602 (1978).
603 5. Hanssen, E. *et al.* Electron tomography of *Plasmodium falciparum* merozoites reveals
604 core cellular events that underpin erythrocyte invasion. *Cell Microbiol* **15**, 1457–72
605 (2013).
606 6. Dubremetz, J. F. Rhoptries are major players in *Toxoplasma gondii* invasion and host
607 cell interaction. *Cell Microbiol* **9**, 841–8 (2007).
608 7. Porchet-Hennere, E. & Nicolas, G. Are rhoptries of Coccidia really extrusomes? *J*
609 *Ultrastruct Res* **84**, 194–203 (1983).

8. Koshy, A. A. *et al. Toxoplasma* co-opts host cells it does not invade. *PLoS Pathog* **8**, e1002825 (2012).
9. Chen, L. *et al.* The *Toxoplasma gondii* virulence factor ROP16 acts in cis and trans, and suppresses T cell responses. *J. Exp. Med.* **217**, (2020).
10. Carruthers, V. B. & Sibley, L. D. Mobilization of intracellular calcium stimulates microneme discharge in *Toxoplasma gondii*. *Mol Microbiol* **31**, 421–8 (1999).
11. Paredes-Santos, T. C., de Souza, W. & Attias, M. Dynamics and 3D organization of secretory organelles of *Toxoplasma gondii*. *J Struct Biol* **177**, 420–30 (2012).
12. Brugerolle, G. *Colpodella vorax*: ultrastructure, predation, life-cycle, mitosis, and phylogenetic relationships. *Europ. J. Protistol.* **38**, 113–125 (2002).
13. Perkins, F. O. Zoospores of the Oyster Pathogen, *Dermocystidium marinum*. I. Fine Structure of the Conoid and Other Sporozoan-Like Organelles. *J. Parasitol.* **62**, 959–974 (1976).
14. Warrenfeltz, S. *et al.* EuPathDB: The Eukaryotic Pathogen Genomics Database Resource. *Methods Mol. Biol. Clifton NJ* **1757**, 69–113 (2018).
15. Aranda, M. *et al.* Genomes of coral dinoflagellate symbionts highlight evolutionary adaptations conducive to a symbiotic lifestyle. *Sci Rep* **6**, 39734 (2016).
16. Katoh, K. & Standley, D. M. MAFFT multiple sequence alignment software version 7: improvements in performance and usability. *Mol Biol Evol* **30**, 772–80 (2013).
17. Dress, A. W. *et al.* Noisy: identification of problematic columns in multiple sequence alignments. *Algorithms Mol Biol* **3**, 7 (2008).
18. Lemoine, F. *et al.* NGPhylogeny.fr: new generation phylogenetic services for non-specialists. *Nucleic Acids Res* **47**, W260–W265 (2019).
19. Lefort, V., Longueville, J. E. & Gascuel, O. SMS: Smart Model Selection in PhyML. *Mol Biol Evol* **34**, 2422–2424 (2017).

635 20. Guindon, S. *et al.* New algorithms and methods to estimate maximum-likelihood
636 phylogenies: assessing the performance of PhyML 3.0. *Syst Biol* **59**, 307–21 (2010).
637 21. Huynh, M. H. & Carruthers, V. B. Tagging of endogenous genes in a *Toxoplasma*
638 *gondii* strain lacking Ku80. *Eukaryot Cell* **8**, 530–9 (2009).
639 22. Sheiner, L. *et al.* A systematic screen to discover and analyze apicoplast proteins
640 identifies a conserved and essential protein import factor. *PLoS Pathog* **7**, e1002392
641 (2011).
642 23. Koshy, A. A. *et al. Toxoplasma* secreting Cre recombinase for analysis of host-
643 parasite interactions. *Nat Methods* **7**, 307–9 (2010).
644 24. Knuepfer, E., Napiorkowska, M., van Ooij, C. & Holder, A. A. Generating conditional
645 gene knockouts in *Plasmodium* - a toolkit to produce stable DiCre recombinase-
646 expressing parasite lines using CRISPR/Cas9. *Sci Rep* **7**, 3881 (2017).
647 25. Lambros, C. & Vanderberg, J. P. Synchronization of *Plasmodium falciparum*
648 erythrocytic stages in culture. *J Parasitol* **65**, 418–20 (1979).
649 26. Donald, R. G. & Roos, D. S. Insertional mutagenesis and marker rescue in a protozoan
650 parasite: cloning of the uracil phosphoribosyltransferase locus from *Toxoplasma*
651 *gondii*. *Proc Natl Acad Sci U A* **92**, 5749–53 (1995).
652 27. Donald, R. G., Carter, D., Ullman, B. & Roos, D. S. Insertional tagging, cloning, and
653 expression of the *Toxoplasma gondii* hypoxanthine-xanthine-guanine
654 phosphoribosyltransferase gene. Use as a selectable marker for stable transformation.
655 *J Biol Chem* **271**, 14010–9 (1996).
656 28. Jones, M. L. *et al.* A versatile strategy for rapid conditional genome engineering using
657 loxP sites in a small synthetic intron in *Plasmodium falciparum*. *Sci. Rep.* **6**, 21800
658 (2016).

29. Suarez, C. *et al.* A lipid-binding protein mediates rhoptry discharge and invasion in *Plasmodium falciparum* and *Toxoplasma gondii* parasites. *Nat Commun* **10**, 4041 (2019).

30. Peng, D. & Tarleton, R. EuPaGDT: a web tool tailored to design CRISPR guide RNAs for eukaryotic pathogens. *Microb. Genomics* **1**, e000033 (2015).

31. Kim, K., Soldati, D. & Boothroyd, J. C. Gene replacement in *Toxoplasma gondii* with chloramphenicol acetyltransferase as selectable marker. *Science* **262**, 911–4 (1993).

32. Crabb, B. S. & Cowman, A. F. Characterization of promoters and stable transfection by homologous and nonhomologous recombination in *Plasmodium falciparum*. *Proc Natl Acad Sci U A* **93**, 7289–94 (1996).

33. Lentini, G. *et al.* Characterization of *Toxoplasma* DegP, a rhoptry serine protease crucial for lethal infection in mice. *PLoS One* **12**, e0189556 (2017).

34. Lentini, G. *et al.* Identification and characterization of *Toxoplasma* SIP, a conserved apicomplexan cytoskeleton protein involved in maintaining the shape, motility and virulence of the parasite. *Cell Microbiol* **17**, 62–78 (2015).

35. Kaur, H. *et al.* An endosomal syntaxin and the AP-3 complex are required for formation and maturation of candidate lysosome-related secretory organelles (mucocysts) in *Tetrahymena thermophila*. *Mol Biol Cell* **28**, 1551–1564 (2017).

36. Cassidy-Hanley, D. *et al.* Germline and somatic transformation of mating *Tetrahymena thermophila* by particle bombardment. *Genetics* **146**, 135–47 (1997).

37. Mochizuki, K. High efficiency transformation of *Tetrahymena* using a codon-optimized neomycin resistance gene. *Gene* **425**, 79–83 (2008).

38. Sparvoli, D. *et al.* Remodeling the Specificity of an Endosomal CORVET Tether Underlies Formation of Regulated Secretory Vesicles in the Ciliate *Tetrahymena thermophila*. *Curr Biol* **28**, 697-710 e13 (2018).

684 39. Bowman, G. R. & Turkewitz, A. P. Analysis of a mutant exhibiting conditional
685 sorting to dense core secretory granules in *Tetrahymena thermophila*. *Genetics* **159**,
686 1605–16 (2001).
687 40. Briguglio, J. S., Kumar, S. & Turkewitz, A. P. Lysosomal sorting receptors are
688 essential for secretory granule biogenesis in *Tetrahymena*. *J Cell Biol* **203**, 537–50
689 (2013).
690 41. Schindelin, J. *et al.* Fiji: an open-source platform for biological-image analysis. *Nat*
691 *Methods* **9**, 676–82 (2012).
692 42. Couvreur, G., Sadak, A., Fortier, B. & Dubremetz, J. F. Surface antigens of
693 *Toxoplasma gondii*. *Parasitology* **97 (Pt 1)**, 1–10 (1988).
694 43. Lamarque, M. H. *et al.* Plasticity and redundancy among AMA-RON pairs ensure host
695 cell entry of *Toxoplasma* parasites. *Nat Commun* **5**, 4098 (2014).
696 44. Mueller, C. *et al.* The *Toxoplasma* protein ARO mediates the apical positioning of
697 rhoptry organelles, a prerequisite for host cell invasion. *Cell Host Microbe* **13**, 289–
698 301 (2013).
699 45. Lamarque, M. *et al.* The RON2-AMA1 interaction is a critical step in moving
700 junction-dependent invasion by apicomplexan parasites. *PLoS Pathog* **7**, e1001276
701 (2011).
702 46. Hehl, A. B. *et al. Toxoplasma gondii* homologue of *Plasmodium* apical membrane
703 antigen 1 is involved in invasion of host cells. *Infect Immun* **68**, 7078–86 (2000).
704 47. El Hajj, H., Lebrun, M., Fourmaux, M. N., Vial, H. & Dubremetz, J. F. Inverted
705 topology of the *Toxoplasma gondii* ROP5 rhoptry protein provides new insights into
706 the association of the ROP2 protein family with the parasitophorous vacuole
707 membrane. *Cell Microbiol* **9**, 54–64 (2007).

48. Mann, T. & Beckers, C. Characterization of the subpellicular network, a filamentous membrane skeletal component in the parasite *Toxoplasma gondii*. *Mol Biochem Parasitol* **115**, 257–68 (2001).

49. Achbarou, A. *et al.* Differential targeting of dense granule proteins in the parasitophorous vacuole of *Toxoplasma gondii*. *Parasitology* **3**, 321–9 (1991).

50. Achbarou, A. *et al.* Characterization of microneme proteins of *Toxoplasma gondii*. *Mol Biochem Parasitol* **47**, 223–33 (1991).

51. Burghaus, P. A. & Holder, A. A. Expression of the 19-kilodalton carboxy-terminal fragment of the *Plasmodium falciparum* merozoite surface protein-1 in Escherichia coli as a correctly folded protein. *Mol Biochem Parasitol* **64**, 165–9 (1994).

52. Collins, C. R., Withers-Martinez, C., Hackett, F. & Blackman, M. J. An inhibitory antibody blocks interactions between components of the malarial invasion machinery. *PLoS Pathog* **5**, e1000273 (2009).

53. Douki, J. B. *et al.* Adhesion of normal and *Plasmodium falciparum* ring-infected erythrocytes to endothelial cells and the placenta involves the rhoptry-derived ring surface protein-2. *Blood* **101**, 5025–32 (2003).

54. Cowan, A. T., Bowman, G. R., Edwards, K. F., Emerson, J. J. & Turkewitz, A. P. Genetic, genomic, and functional analysis of the granule lattice proteins in *Tetrahymena* secretory granules. *Mol. Biol. Cell* **16**, 4046–4060 (2005).